NASA/CR–2014-218157

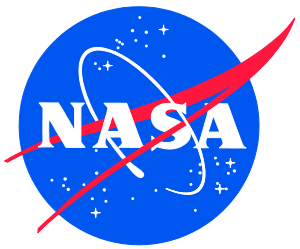

Multilayer Pressure Vessel Materials Testing and Analysis

Phase 1

Joseph W. Cardinal, Carl F. Popelar, and Richard A. Page
Southwest Research Institute, San Antonio, Texas

January 2014

NASA STI Program . . . in Profile

Since its founding, NASA has been dedicated to the advancement of aeronautics and space science. The NASA scientific and technical information (STI) program plays a key part in helping NASA maintain this important role.

The NASA STI program operates under the auspices of the Agency Chief Information Officer. It collects, organizes, provides for archiving, and disseminates NASA's STI. The NASA STI program provides access to the NASA Aeronautics and Space Database and its public interface, the NASA Technical Report Server, thus providing one of the largest collections of aeronautical and space science STI in the world. Results are published in both non-NASA channels and by NASA in the NASA STI Report Series, which includes the following report types:

- TECHNICAL PUBLICATION. Reports of completed research or a major significant phase of research that present the results of NASA Programs and include extensive data or theoretical analysis. Includes compilations of significant scientific and technical data and information deemed to be of continuing reference value. NASA counterpart of peer-reviewed formal professional papers, but having less stringent limitations on manuscript length and extent of graphic presentations.

- TECHNICAL MEMORANDUM. Scientific and technical findings that are preliminary or of specialized interest, e.g., quick release reports, working papers, and bibliographies that contain minimal annotation. Does not contain extensive analysis.

- CONTRACTOR REPORT. Scientific and technical findings by NASA-sponsored contractors and grantees.

- CONFERENCE PUBLICATION. Collected papers from scientific and technical conferences, symposia, seminars, or other meetings sponsored or co-sponsored by NASA.

- SPECIAL PUBLICATION. Scientific, technical, or historical information from NASA programs, projects, and missions, often concerned with subjects having substantial public interest.

- TECHNICAL TRANSLATION. English-language translations of foreign scientific and technical material pertinent to NASA's mission.

Specialized services also include organizing and publishing research results, distributing specialized research announcements and feeds, providing information desk and personal search support, and enabling data exchange services.

For more information about the NASA STI program, see the following:

- Access the NASA STI program home page at *http://www.sti.nasa.gov*

- E-mail your question to help@sti.nasa.gov

- Fax your question to the NASA STI Information Desk at 443-757-5803

- Phone the NASA STI Information Desk at 443-757-5802

- Write to:
  STI Information Desk
  NASA Center for AeroSpace Information
  7115 Standard Drive
  Hanover, MD 21076-1320

NASA/CR–2014-218157

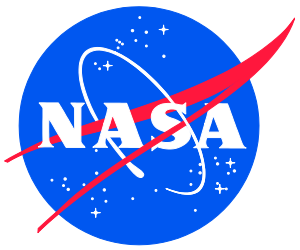

Multilayer Pressure Vessel Materials Testing and Analysis

Phase 1

Joseph W. Cardinal, Carl F. Popelar, and Richard A. Pageaffiliation
Southwest Research Institute, San Antonio, Texas

National Aeronautics and
Space Administration

Langley Research Center
Hampton, Virginia 23681-2199

Prepared for Langley Research Center
under Contract NNA09DB39C

January 2014

Acknowledgments

The authors of this report would like to first express their appreciation to Mr. Doug Fraser of NASA Ames Research Center for supplying key background information on the AO Smith multilayer pressure vessel along with related "legacy" reports and documents. Secondly, Mr. Steve Ziola of Digital Wave Corporation is acknowledged for providing information and data on the conduct of the cyclic pressure testing as well as coordinating the shipment of the pressure vessel to Southwest Research Institute (SwRI).

Special thanks are due to Mr. Doyle Smith and his supporting cast of welders in SwRI's Fabrication Shop for carefully sectioning the vessel into smaller pieces for material testing. The technical staff of the solids and metallurgical labs are acknowledged for their support of the material characterization testing and the failure analysis. Finally, Ms. Deborah Gohmert and Ms. Alberta Matthews are acknowledged for the preparation of the final report.

Available from:

NASA Center for AeroSpace Information
7115 Standard Drive
Hanover, MD 21076-1320
443-757-5802

LIST OF REVISED PAGES

Multilayer Pressure Vessel Materials

Testing and Analysis (Phase 1)

SwRI Project 18.17408

Table One

Revision Number	Issue Date
Final Report	September 20, 2012
Revision 1	November 6, 2012

Issue dates for the original document and all subsequent changes are given in Table One. Table Two lists all pages affected by the latest revision or by any previously issued revision. Pages not listed in Table Two are the same as issued with the original document. All pages affected by a revision are annotated with the words "Revision ____" with the underscore replaced by the pertinent Revision Number as given in Table Two. This annotation will be printed immediately to the right of the page number at the bottom of the revised page.

Table Two

Revision No.	Page No	Description
1	3-1	text revisions; material grades added
1	4-1	text revisions
1	5-1	text revisions; footnote #2 added
1	5-2	text revisions; footnote #3 added
1	5-3	lateral expansion data added to Table 5-2
1	5-7	text revisions
1	5-11	text revisions
1	5-15	text revisions
1	5-16	text revisions
1	6-1	heading correction
1	7-2	text revisions

TABLE OF CONTENTS

LIST OF FIGURES

LIST OF TABLES

EXECUTIVE SUMMARY

To provide the National Aeronautics and Space Administration (NASA) a comprehensive suite of materials strength, fracture toughness and crack growth rate test results for use in remaining life calculations for aging multilayer pressure vessels, Southwest Research Institute® (SwRI®) was contracted in two phases to obtain relevant material property data from a representative vessel. This report describes Phase 1 of this effort which includes a preliminary material property assessment as well as a fractographic, fracture mechanics and fatigue crack growth analyses of an induced flaw in the outer shell of a representative multilayer vessel that was subjected to cyclic pressure test. SwRI performed this Phase 1 effort under contract to the Digital Wave Corporation in support of their contract to Jacobs ATOM for the NASA Ames Research Center.

A multilayer AO Smith pressure vessel was shipped to SwRI and was torch cut into smaller sections to facilitate excising samples for material test coupons. This Phase 1 effort used only a small portion of the vessel material for material characterization testing. The remainder of the vessel sections are being retained in storage at SwRI for use in the more detailed material characterization effort underway in the Phase 2 program. Samples for chemical analysis were removed from the head and the shell of the vessel. The results obtained from the chemical analyses of the head and shell materials are presented in Section 3.0 and are compared with AISI and ASTM specifications.

Section 4.0 of this report provides a detailed fractographic analysis of the notch and crack that was located in the outer shell layer during the cyclic pressure test performed by the Digital Wave Corporation. This analysis indicated that a fatigue crack initiated from the notch and eventually grew to a depth where the crack rapidly fractured through the remaining ligament.

Section 5.0 summarizes the results of some basic mechanical testing that was performed in order to characterize the mechanical behavior of the AO Smith 1146a shell and A-225 Grade B head materials. This characterization is an initial portion of a more comprehensive effort (Phase 2) to characterize the pressure vessel constituents, including the heads, inner and outer shells and the welds (shell seam welds and head-to-shell girth welds). Results are presented for tensile tests, Charpy tests, fracture toughness tests, and fatigue crack growth rate tests. A number of key conclusions resulting from this Phase 1 testing effort are provided in Section 5.6. Based on these results, considerations and recommendations for the ongoing Phase 2 effort are provided in Section 5.7.

Sections 6.0 and 7.0 provide fracture mechanics and fatigue crack growth analyses of the crack that grew out of the notch during the vessel cyclic pressure test. The analyses were performed using the NASGRO® software. These analyses use the test data generated in this program and produce reasonable agreement with the observations made from the analysis of the fracture surface presented in Section 4.0 and compare well with the numbers of pressure cycles applied to the vessel during the test at Digital Wave.

1.0 INTRODUCTION

The National Aeronautics and Space Administration (NASA) owns and operates several hundred multi-layer pressure vessels, some of which are more than fifty years old. While available construction records show that generally good design, fabrication, and inspection processes were followed, these vessels are non-Code vessels and actual records do not exist for many of these vessels. Furthermore, the materials used typically correspond to a proprietary manufacturer's specification (not an ASME or ASTM material grade). In addition, due to their age and operating history, it is possible that cracks have developed over time and could provide a potential failure mechanism during future operation. Therefore, in order to ensure the safe future operation of these vessels, it is necessary to obtain accurate material properties such as strength, fracture toughness and fatigue crack growth rate data.

To provide NASA a comprehensive suite of materials strength, fracture toughness and crack growth rate test results for use in remaining life calculations for the vessels described above, Southwest Research Institute (SwRI) was contracted in two phases to obtain relevant material property data from a representative vessel. This report describes Phase 1 of this effort which includes a preliminary material property assessment as well as a fractographic, fracture mechanics and fatigue crack growth analyses of an induced flaw in the outer shell of the representative multi-layer vessel.

The vessel from which material was taken was manufactured by AO Smith in 1959 (serial number MV50466-8) and the name plate is shown in Figure 1-1. It is nominally 36.25 inches in outside diameter and approximately 7 feet 4 inches long. The head is nominally 2.5 inches thick and the shell is comprised of twelve layers with the inner (first) layer 3/8-inch thick and the remaining eleven layers each 1/4-inch thick giving a total nominal wall thickness of 3.125 inches. This vessel had undergone cyclic pressure testing in an attempt to monitor fatigue crack growth from induced flaws using Modal Acoustic Emissions (MAE) Non-destructive Examination (NDE) by the Digital Wave Corporation (DW). This vessel was not ASME Code stamped, and AO Smith used proprietary, non-ASME materials specifications for the shell and nozzles. The heads were fabricated from a standard ASTM material.

The intent of this Phase 1 testing program was to perform a preliminary characterization of the strength, fracture and fatigue crack growth properties of the vessel shell (outer layer) and the head parent material using current ASTM standard test methods. The AO Smith and ASTM material specifications were to be compared to for reference. In addition, the single flaw that was deemed to have exhibited some fatigue crack growth during the cyclic pressure testing and MAE monitoring was to be analyzed fractographically. Fracture mechanics and fatigue crack growth analyses of this flaw were also to be performed using the NASGRO® software and the data generated in this Phase 1 effort in order to demonstrate the ability to perform remaining safe service life assessments on similar vessels. The results of this Phase 1 effort were also to be used to provide guidance for the much more extensive material property characterization effort planned in Phase 2.

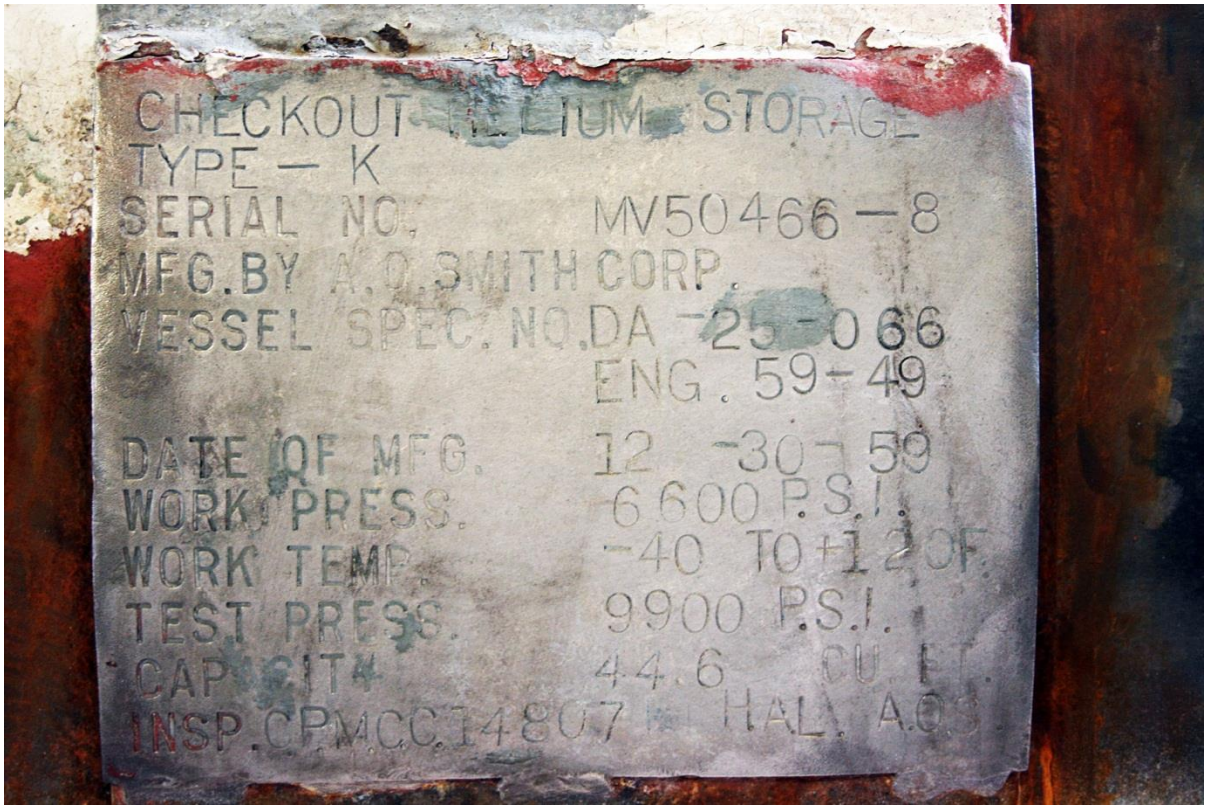

Figure 1-1. Nameplate from AO Smith Multi-Layer Pressure Vessel (MV50466-8)

2.0 VESSEL SECTIONING

The multi-layer AO Smith pressure vessel was shipped to SwRI in late April 2012 and was unloaded at the Structural Engineering Department's Fabrication Shop (see Figure 2-1). As a precautionary measure, it was assumed that the paint on the vessel contained lead and the vessel was stripped of all paint by an outside vendor capable of safely containing and disposing of the paint before any sectioning was performed.

Using AO Smith drawing number MV50466, a vessel sectioning plan was developed and is shown in Figure 2-2. The vessel was torch cut approximately along the red dotted lines in Figure 2-2 and then subsequently the shell and the head-to-shell weld were cut into smaller sections to facilitate excising samples for material test coupons. Special care was taken to protect the crown area of the outer shell that contained the notch (flaw) that was monitored by MAE during the cyclic pressure testing of the vessel. Figure 2-3 shows a number of photos of the vessel segments that resulted after the transverse cuts were made. The center section of the shell was then quartered as was one of the rings containing the head-to-shell weld. Photos of some of these sections are shown in Figure 2-4. A cross-section through the head-to-shell weld is shown in Figure 2-5.

One of the most notable observations from the vessel sectioning process was how tight the layers of the shell were in contact with each other; see the photo in the upper right hand corner of Figure 2-3 and Figure 2-5. However, once the shell ring was cut axially, the layers sprung apart loosely as shown in Figure 2-4. In flipping through one of the stacks of shell layers, a Carilloy Steel logo was found on layer number nine (assuming the inside layer is layer number one) as shown in Figure 2-4. This was indeed a surprise to see and indicates that the source of the steel that AO Smith used for the layers of the shell was Carilloy Steel, which at the time, was a subsidiary of US Steel.

This Phase 1 effort used only a small portion of the vessel material for material characterization testing. The remainder of the vessel sections are being retained in storage at SwRI for use in the more detailed material characterization effort underway in the Phase 2 program.

Figure 2-1. Vessel Arrival at SwRI's Fabrication Shop

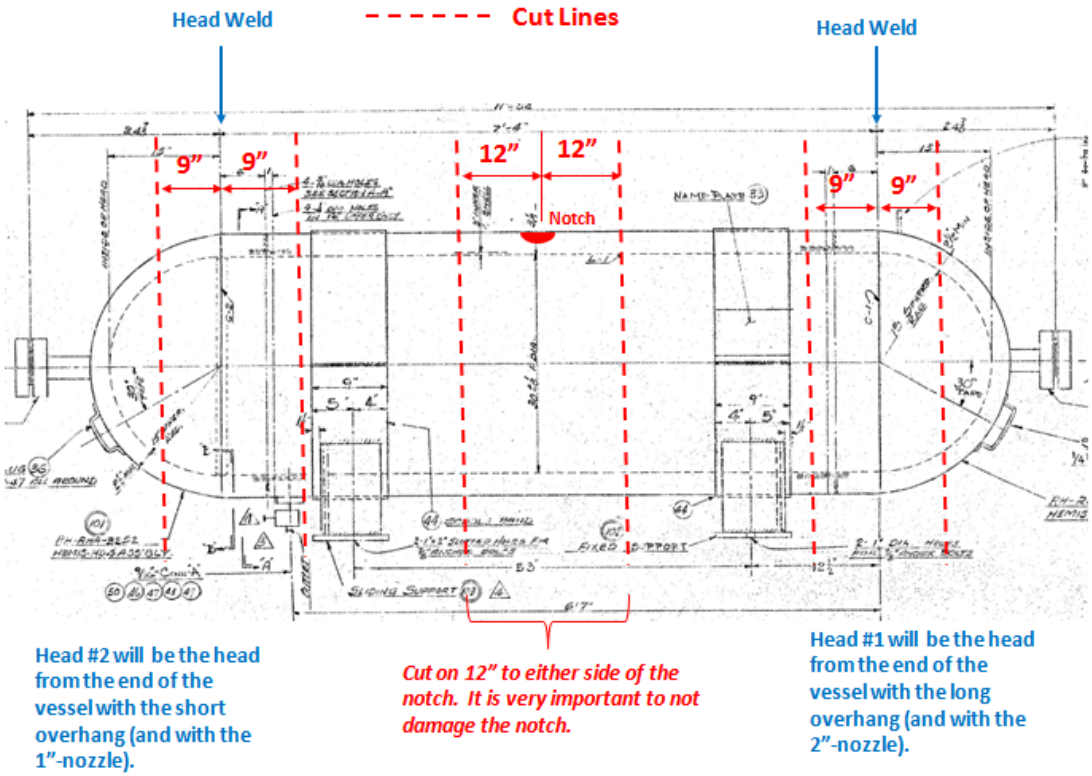

Figure 2-2. Vessel Sectioning Plan (Approximate Dimensions; Notch not to Scale)

Figure 2-3. Photos of Sectioned Pressure Vessel

Figure 2-4. Photos of Shell Layers and Carilloy Steel Logo

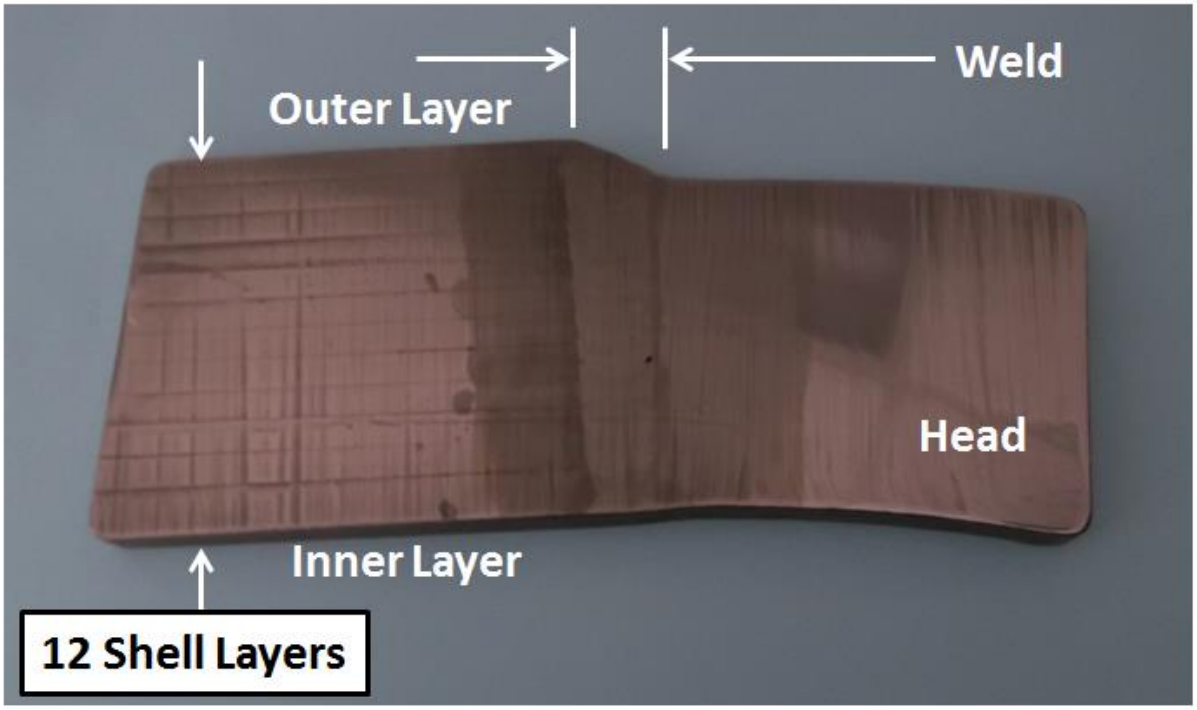

Figure 2-5. Cross-section Through Head-to-Shell Weld Showing Shell Layers

3.0 CHEMICAL ANALYSIS

Samples for chemical analysis were removed from the head and the shell of the vessel. The results obtained from the chemical analyses of the head and shell materials are listed in Table 3-1. The head material satisfies the composition specifications for AISI 1513 and 1522 high manganese carbon steel and the shell material meets the specifications for AISI 1522 and 1524 high manganese carbon steel[1]. The shell material also meets the composition requirements of ASTM A-299 and A-225, Grade C[2]. The head material, which was reportedly A-225 Gr. B, contains less nickel than listed in the 1999 specification for A-225; however, it does meet the A-299[2] specifications and the A-225 Gr. B specifications that were in place in 1956. The shell material also meets AO Smith's 1146a specification, while the head material falls below this specification in both carbon and nickel content. For reference, the AISI, ASTM, and AO Smith specifications are also listed in Table 3-1.

Table 3-1. Chemical Composition of Head and Shell Material

Material	Composition, wt.%										
	C	Mn	P	S	Si	Ni	Cr	Mo	Cu	V	Al
Head	0.16	1.40	0.033	0.028	0.20	0.20	0.19	0.02	0.02	NM[4]	<0.01
Shell	0.21	1.36	0.025	0.018	0.26	0.53	0.07	0.01	0.04	NM[4]	0.05
AISI 1513	0.10-0.	1.1-1.4	0.040 max	0.050 max	—	—	—	—	—	—	—
AISI 1522	0.18-0.	1.1-1.4	0.040 max	0.050 max	—	—	—	—	—	—	—
AISI 1524	0.19-0.	1.35-1.	0.040 max	0.050 max	—	—	—	—	—	—	—
ASTM A-225 Gr. C[2]	0.25 max	1.72 max	0.035 max	0.035 max	0.13-0.	0.37-0.73	—	—	—	0.11-0.20	—
ASTM A-299[2]	0.28 max	0.84-1.	0.035 max	0.035 max	0.13-0.	—	—	—	—	—	—
ASTM A-225 Gr. B[3]	0.20 max	1.45 max	0.04 max	0.05 max	0.15-0.					0.09-0.14	
AO Smith 1146a	0.18-0.	1.10-1.	0.04 max	0.05 max	0.20-0.	0.40-0.70				0.13-0.18	

[1] When the composition of an element such as nickel is not specified, concentrations in the range of 0.2 to 0.5 wt.% are considered to be within specification as non-deliberate additions.

[2] 1999 vintage ASTM specification

[3] 1956 vintage ASTM specification

[4] Not measured

4.0 FRACTOGRAPHY OF CRACK FROM NOTCH IN OUTER SHELL

A 4½ inch wide section containing the notch was excised from the vessel shell. Two triangular sections were then removed from the section on either end of the notch such that a ½ inch long ligament was present on each end. An impact force, which applied a bending stress across the notch, was then applied to produce a room temperature fracture of the intact ligaments.

A photograph of one face of the opened notch is provided in Figure 4-1. The notch is the dark grey, thumbnail shaped feature along the top of the opened face. The light grey regions on either end of the notch are the lab fracture. The narrow, medium grey, thumbnail shaped region directly below the notch appears to be a fatigue crack that grew from the notch. The medium grey region beneath the fatigue crack appears to be a region of rapid fracture.

The notch was 2.01 inch long and 0.172 inch deep. The fatigue crack was 1.78 inch long and 0.06 inch deep. A 0.03 inch ligament was present between the tip of the fatigue crack and the inner surface of the plate. The thickness of the shell was nominally 0.26 inches.

While the notch was covered with a dark grey oxide, both the fatigue crack and the region of rapid fracture were covered with medium grey colored oxides. Isolated regions of rust colored oxides were also present on all three surfaces. A backscattered electron image of the transition from the fatigue crack to the rapid fracture is provided in Figure 4-2. Patches of thicker oxides are evident in this image. Energy dispersive x-ray spectroscopy (EDS) was used to determine the chemical composition of these oxides. The EDS spectrum, shown in Figure 4-3, indicates that the oxides contained large concentrations of Si and O and smaller amounts of Na, Al, S, K, Ca, and Fe.

An ENDOX® process was used to remove the oxides from the fracture surface without altering the underlying fracture surface features. A stereomicroscope image of the opened crack following cleaning is presented in Figure 4-4. The fatigue crack exhibited bands oriented along the plane of the plate but no evidence of beach marks that would indicate significant changes in the fatigue loading, as shown in Figure 4-5.

Following the stereomicroscope examination, the fracture surface was examined in a scanning electron microscope (SEM). A montage of low magnification SEM images of the fracture surface is provided in Figure 4-6. The locations of each of the higher magnification images that follow are indicated numerically on the image. The bands along the plate plane that were observed in the stereomicroscope appeared as seams in the plate in the SEM, as shown in Figure 4-7. Although the microstructure of the plate was not examined, these seams are likely the result of laminar slag inclusions that were elongated during the rolling process. The images taken from various regions of the fatigue crack are shown in Figures 4-8 through 4-13. Regions of fatigue striations were evident at multiple locations, as shown in Figures 4-8, 4-11, 4-12, and 4-13. Crack growth rate estimates obtained from the striation spacings ranged from 7.2×10^{-6} inch/cycle near the notch to 1.8×10^{-5} inch/cycle adjacent to the transition to fast fracture. While most of the fracture was transgranular, isolated regions of intergranular fracture were present, as shown in Figures 4-9, 4-10, and 4-11. Secondary (out of plane) cracking was also evident, as seen in Figures 4-10, 4-11, 4-12, and 4-13.

Dimpled cup and cone features representative of a ductile fracture process were present throughout the rapid fracture region, as shown in Figures 4-14 through 4-17. Virtually identical dimple features were present in the regions of laboratory fracture, as shown in Figure 4-18.

In summary, the fractographic features that were revealed by opening the notch indicate that a fatigue crack initiated from the notch and grew to a length of 1.78 inch and a depth of 0.064 inch. At this size, the loading applied to the crack was sufficient to produce rapid crack advance, which appears to have propagated the crack through the wall. Note that the fatigue crack grew primarily in the depth (thickness) direction and did not grow lengthwise outside of the notch.

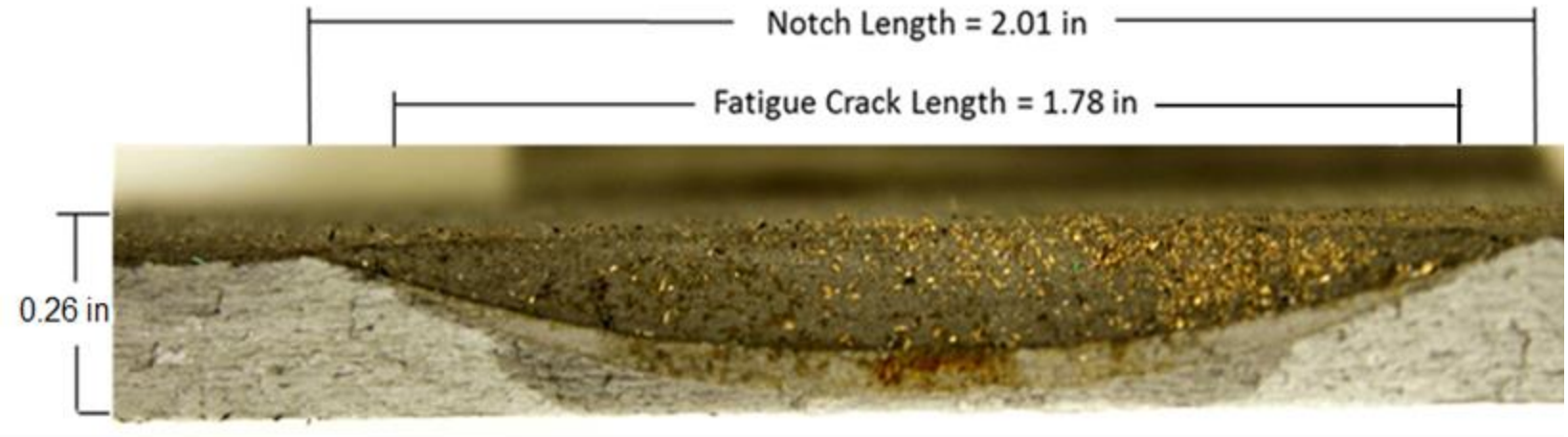

Figure 4-1. Photograph of One Face of the As-Opened Crack

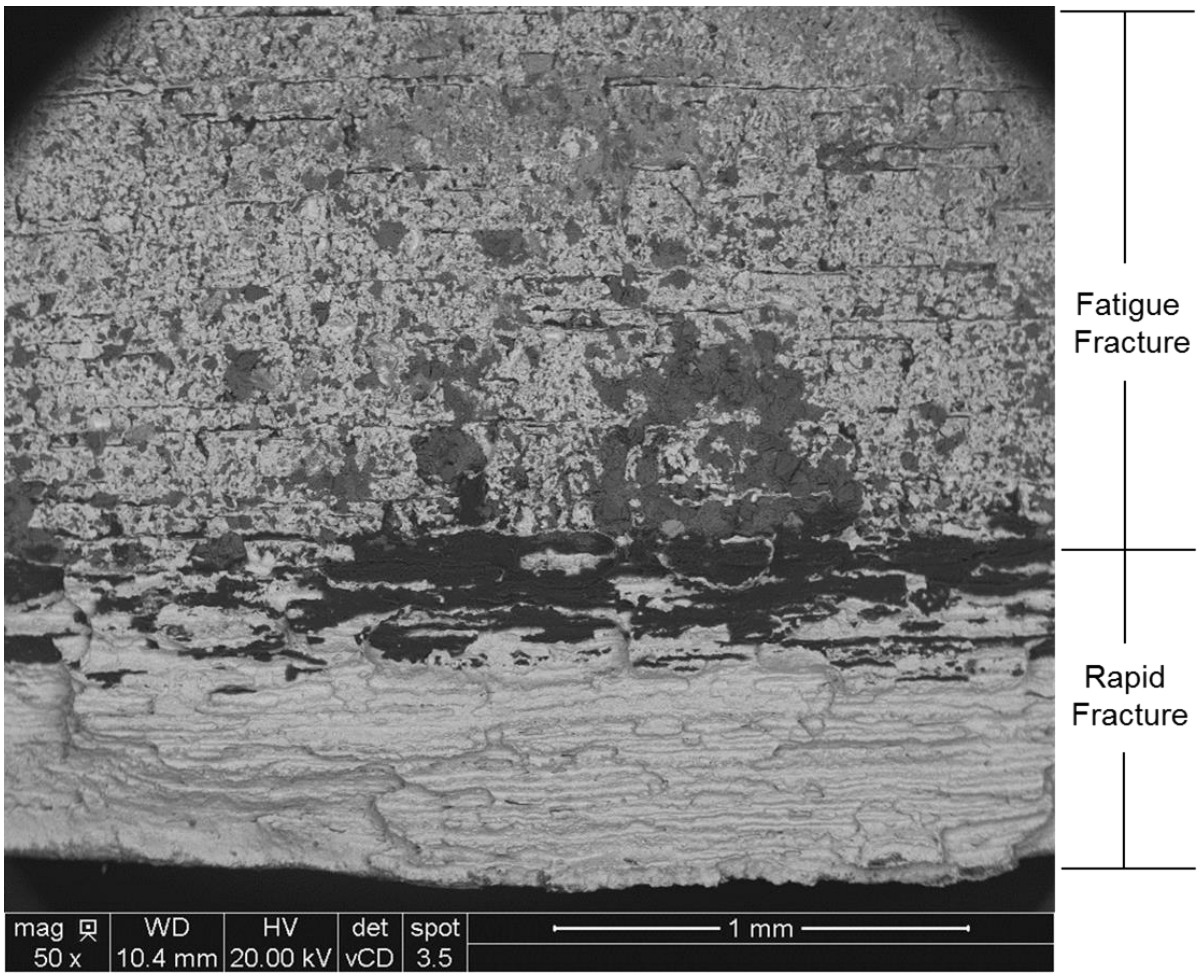

Figure 4-2. SEM Image of Deposits Present on the As-Opened Crack

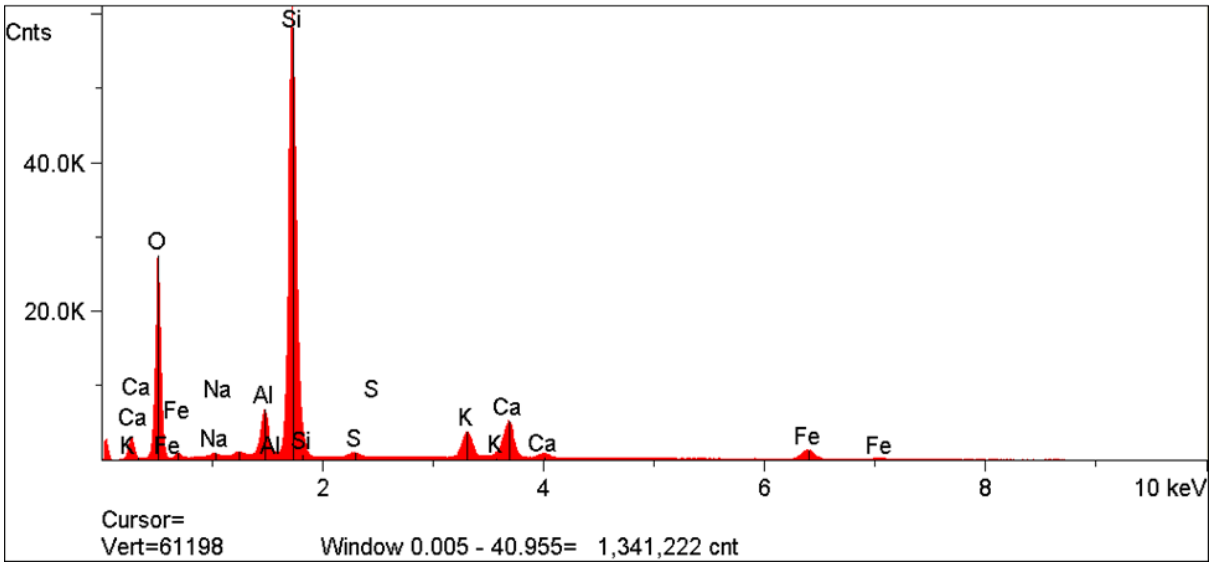

Figure 4-3. EDS Spectrum from Deposits Present of the Crack Surface

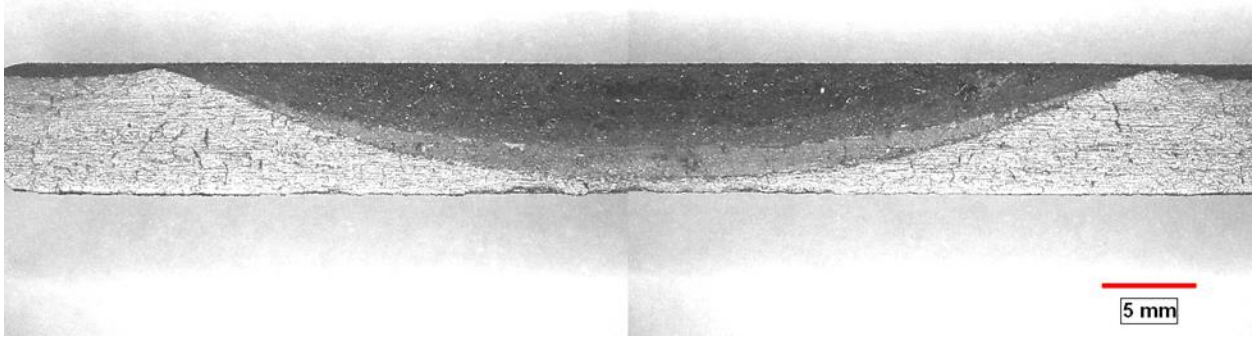

Figure 4-4. Low Magnification Stereomicroscope Image of One Face of the Opened Crack

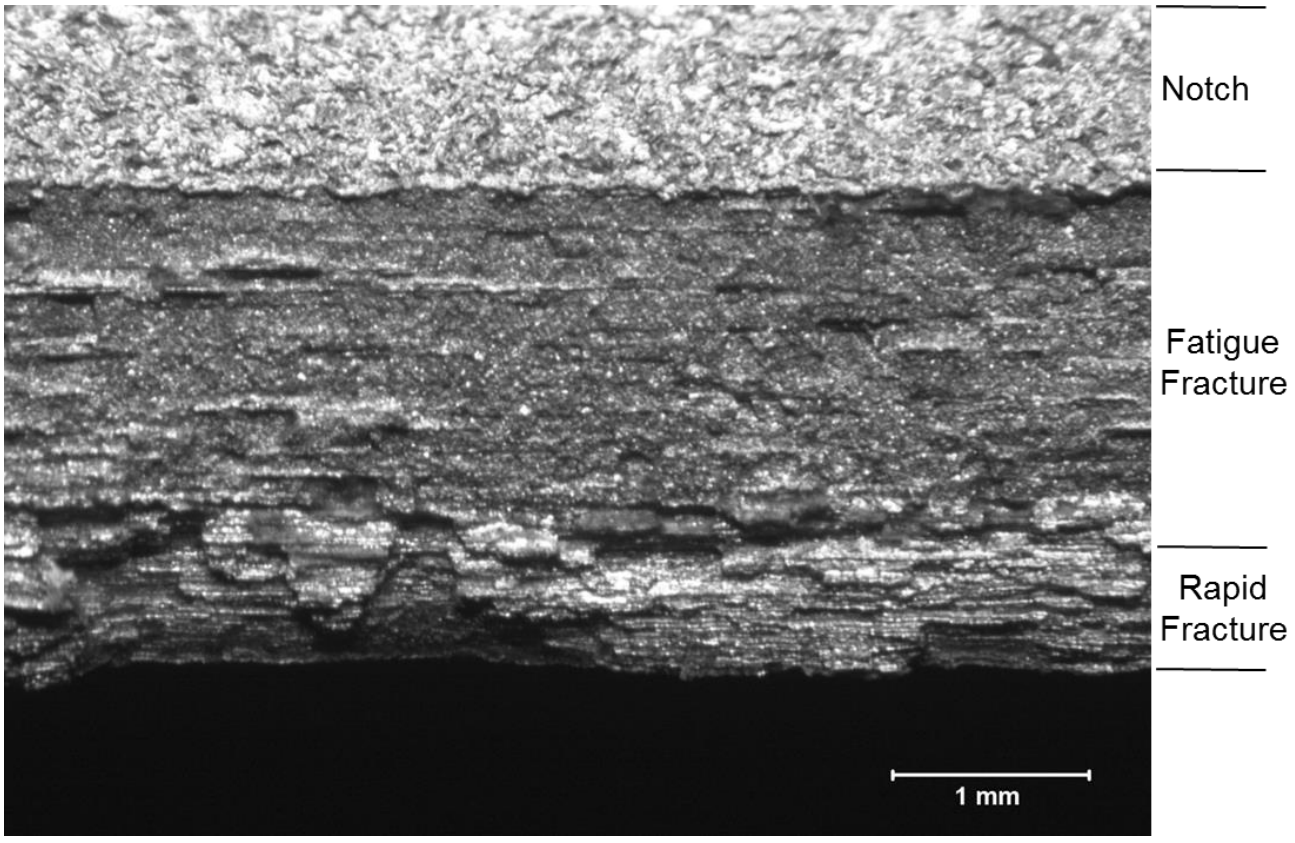

Figure 4-5. Higher Magnification Stereomicroscope Image of the Center of the Opened Crack

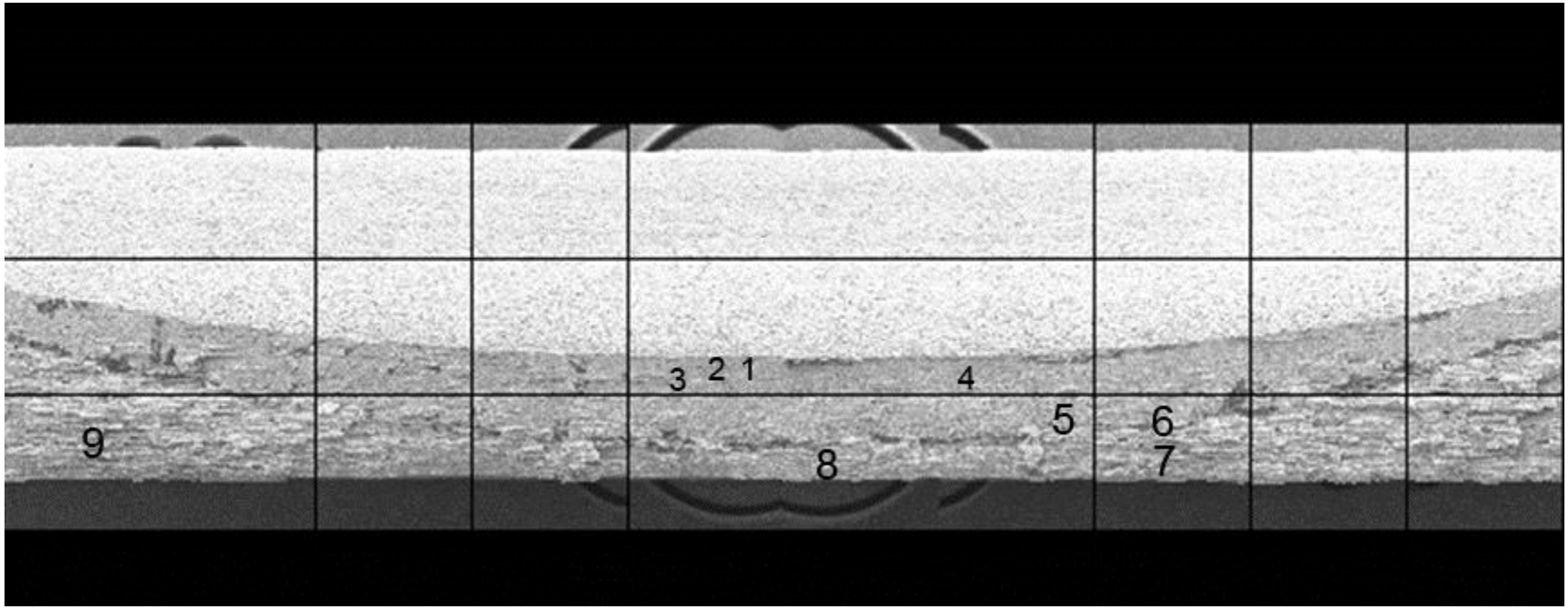

Figure 4-6. Montage of Low Magnification SEM Images of the Center of the Opened Crack

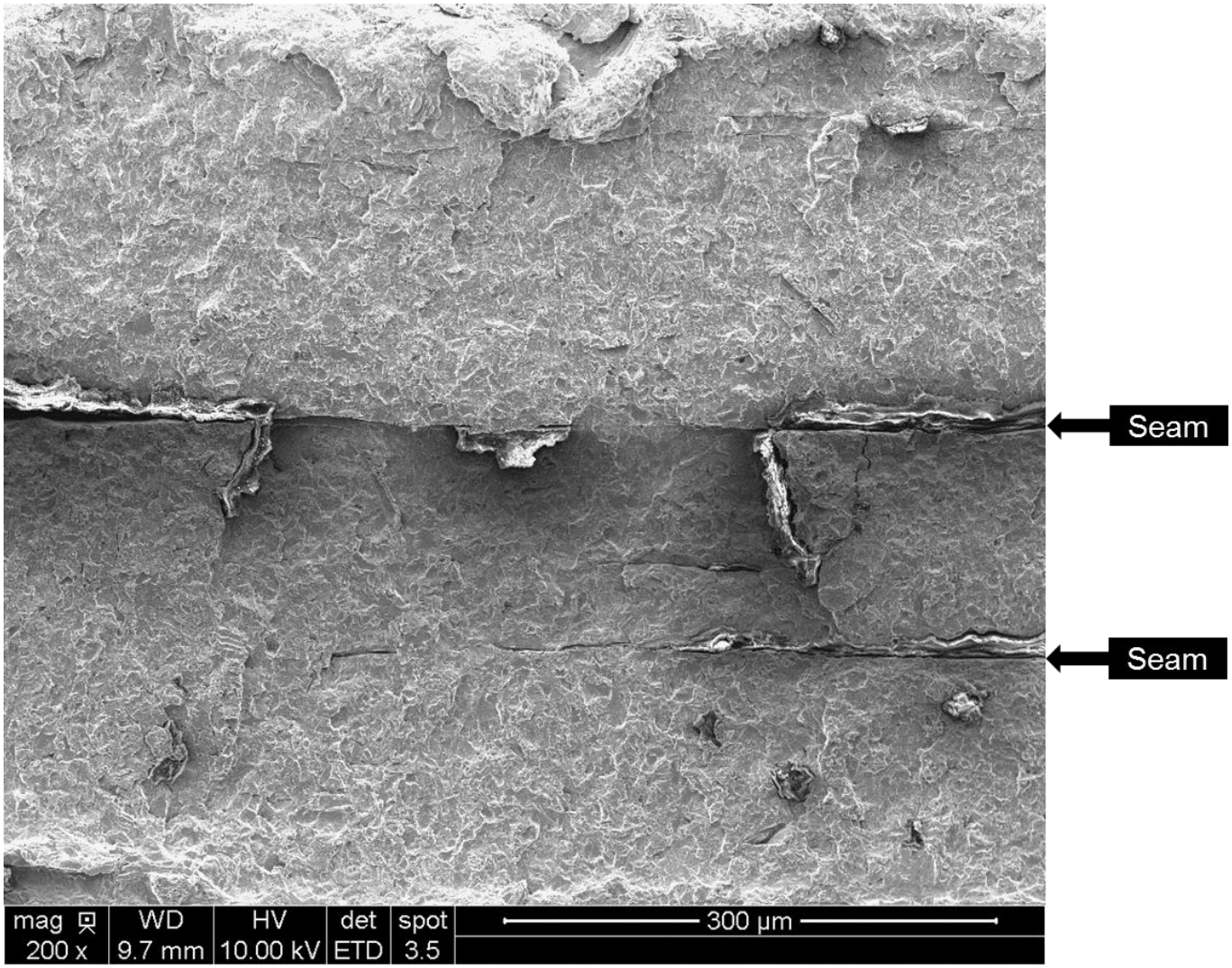

Figure 4-7. Low Magnification SEM Image of Location 1 in Figure 4-6

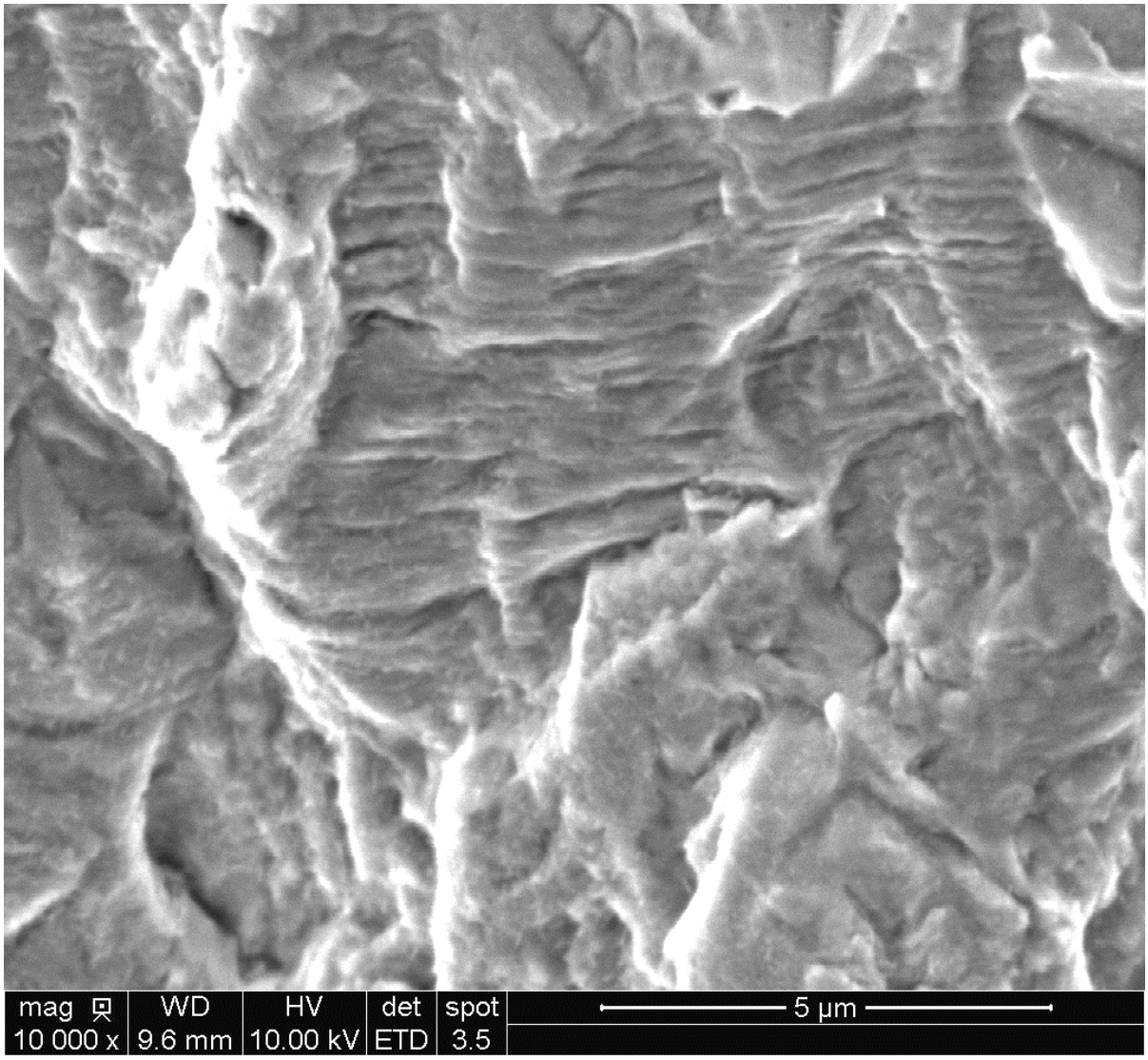

Figure 4-8. SEM Image of Fatigue Striations at Location 1 in Figure 4-6.

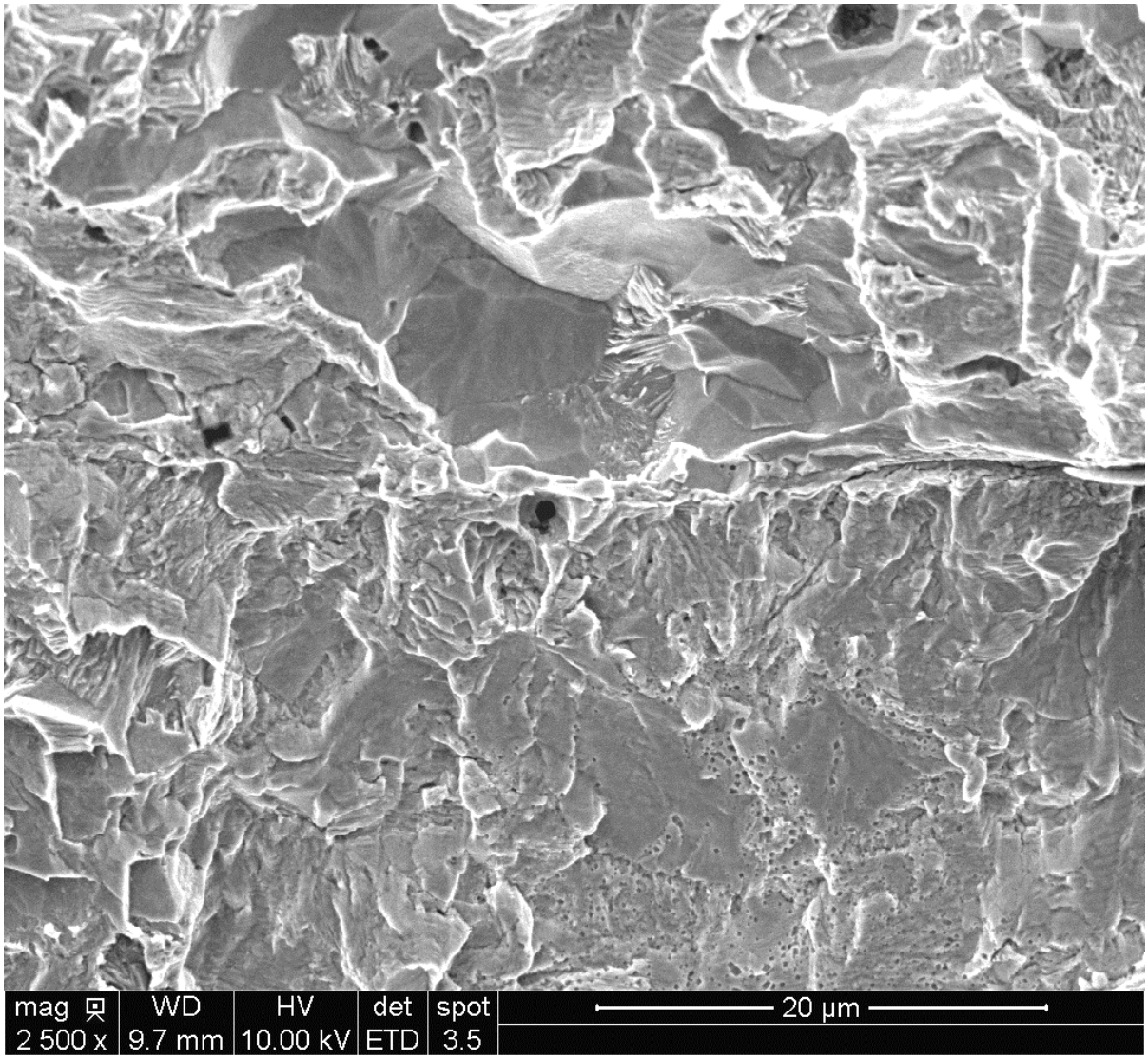

Figure 4-9. SEM Image of Isolated Intergranular Fracture Features at Location 2 in Figure 4-6.

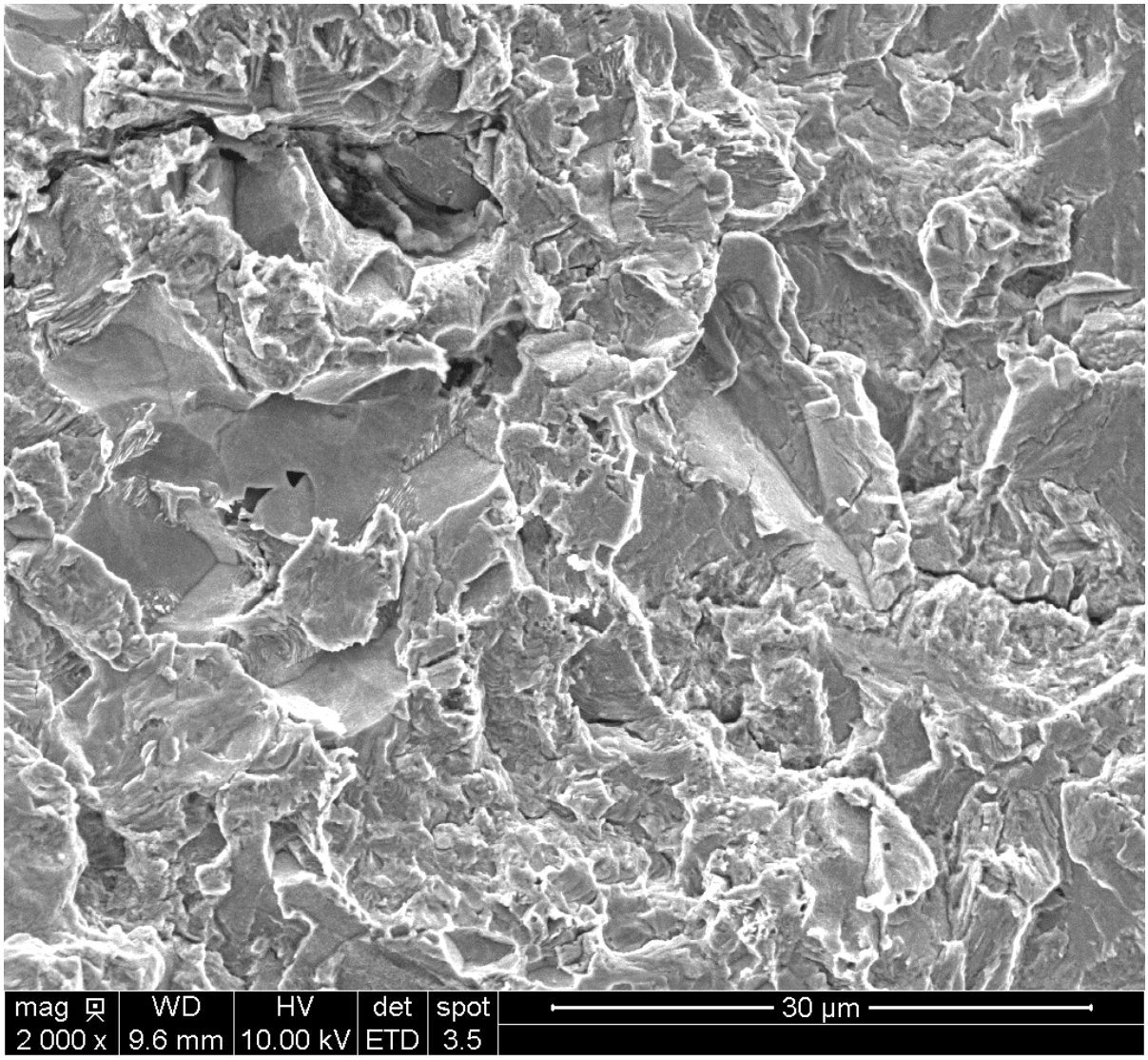

Figure 4-10. SEM Image of Isolated Intergranular Fracture Features and Secondary Cracking at Location 3 in Figure 4-6

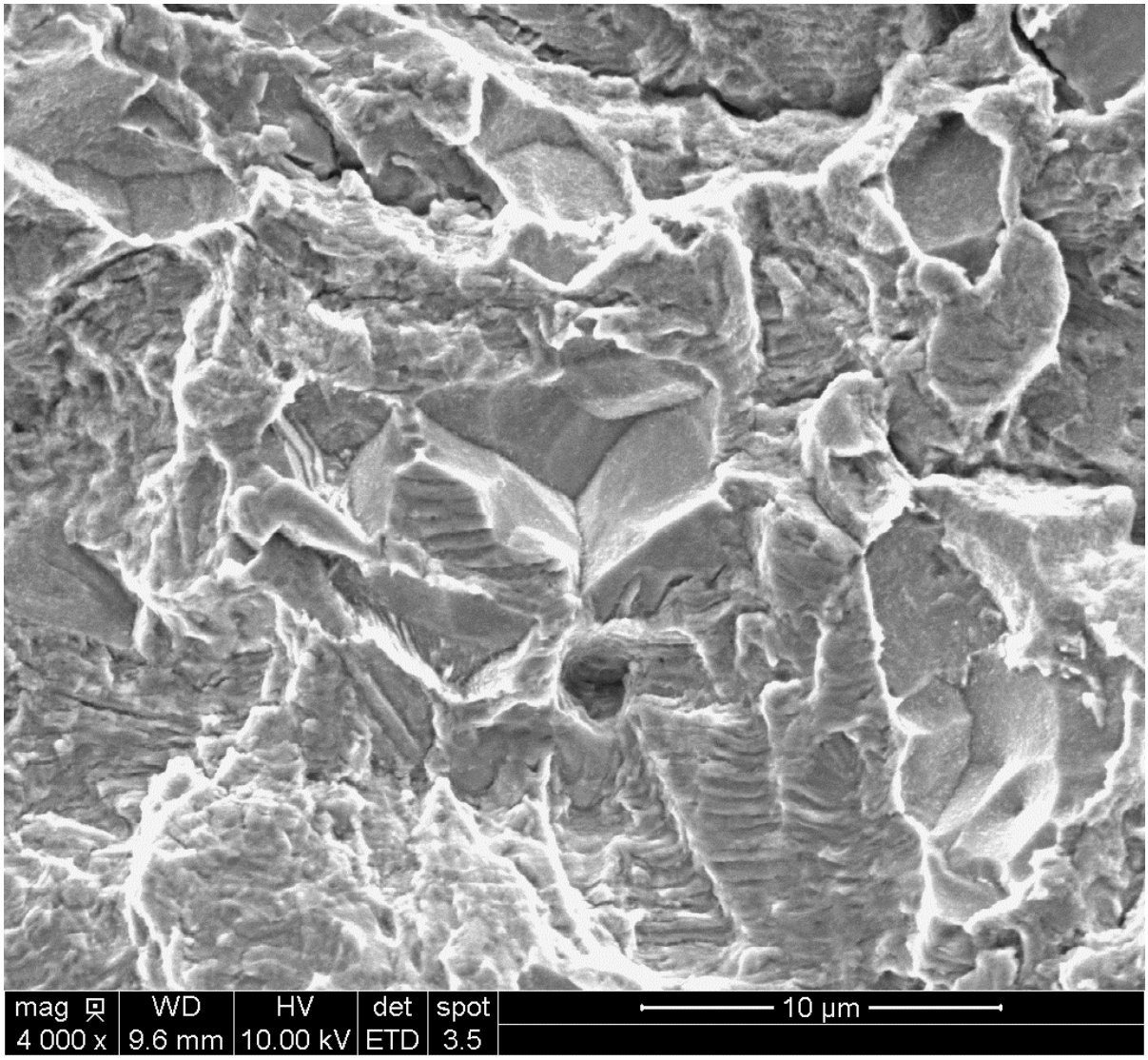

Figure 4-11. SEM Image of Fatigue Striations and Intergranular Fracture Features at Location 3 in Figure 4-6

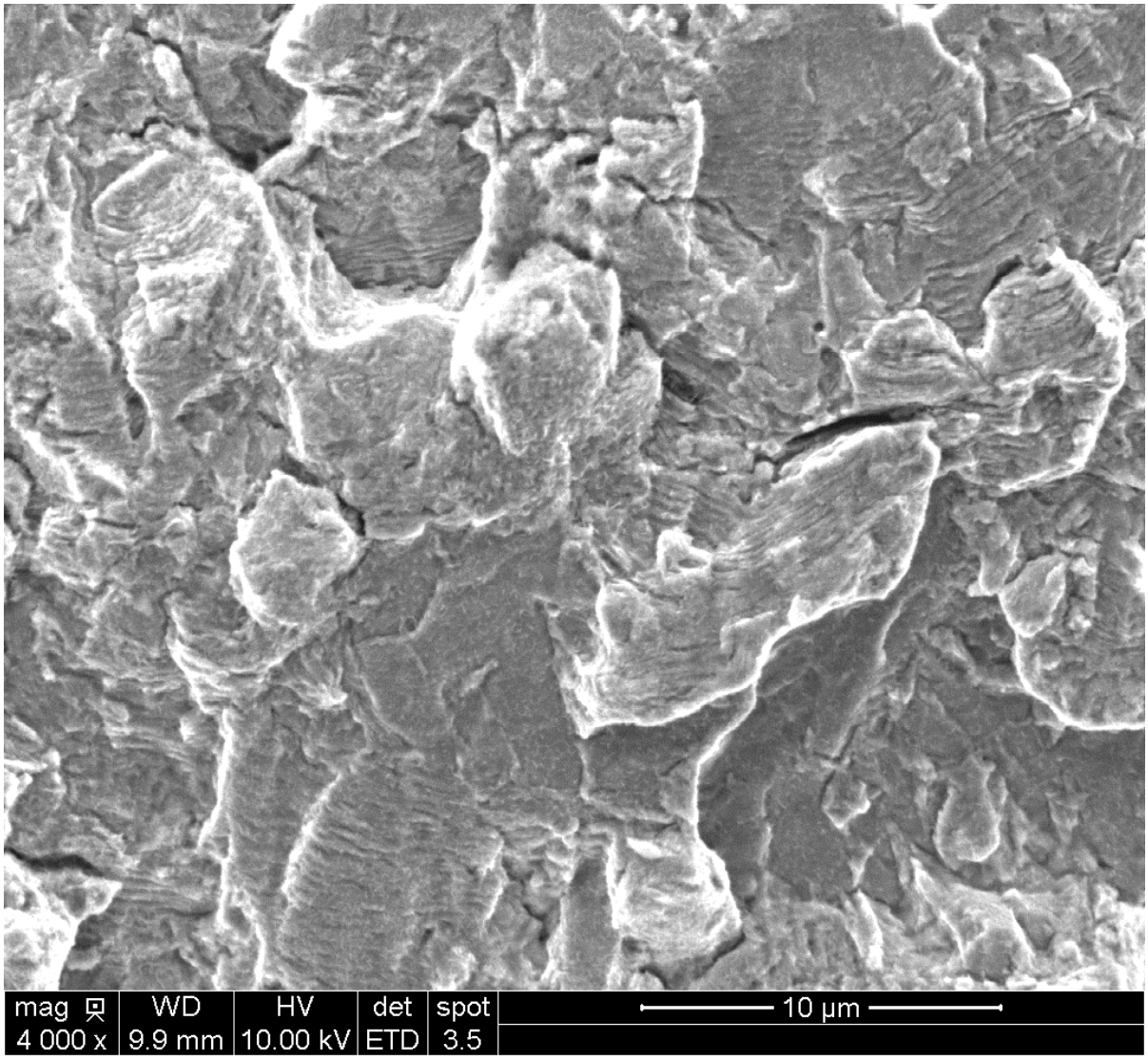

Figure 4-12. SEM Image of Fatigue Striations and Secondary Cracking at Location 4 in Figure 4-6

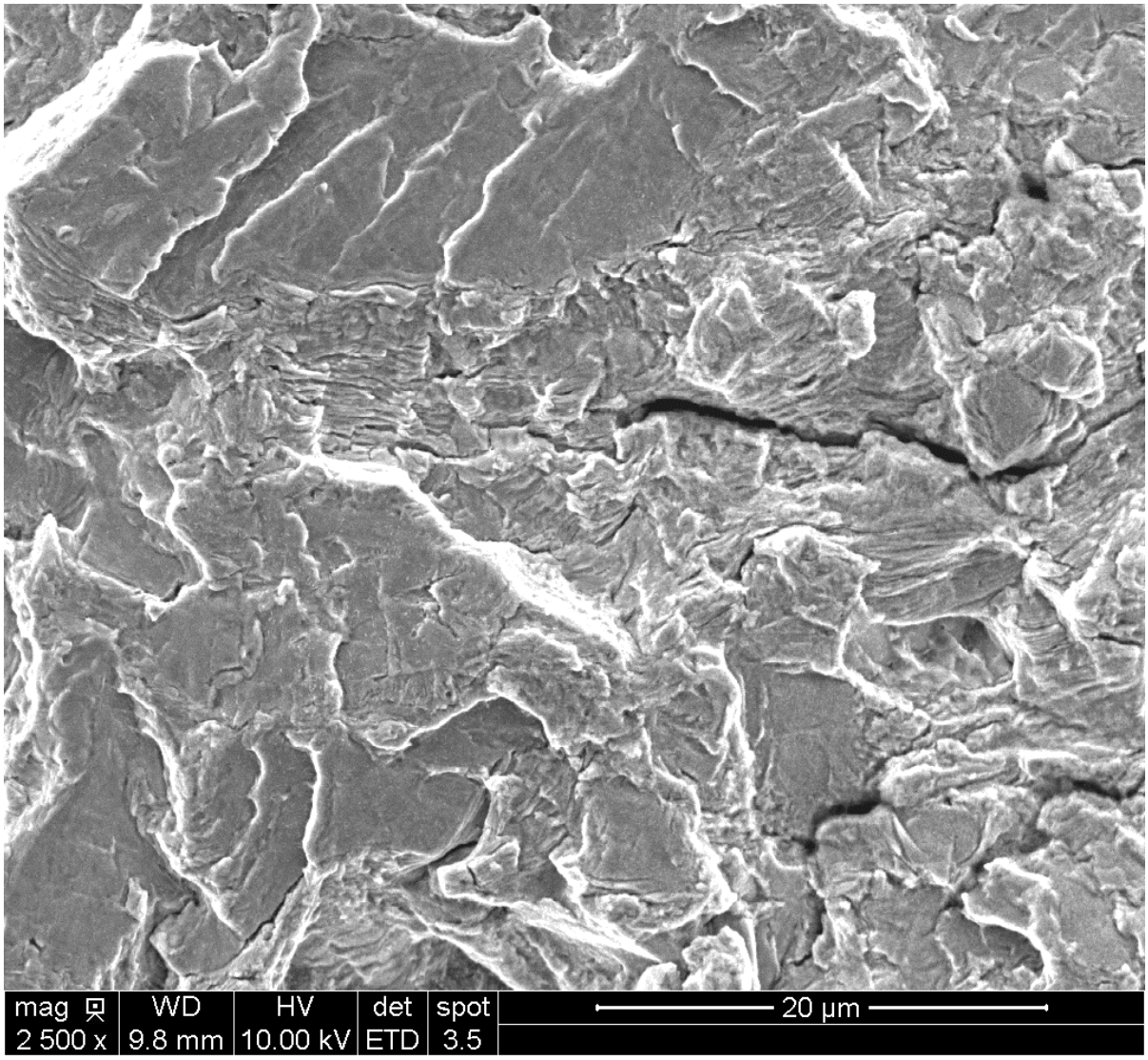

Figure 4-13. SEM Image of Transgranular Fracture, Fatigue Striations, and Secondary Cracking at Location 5 in Figure 4-6

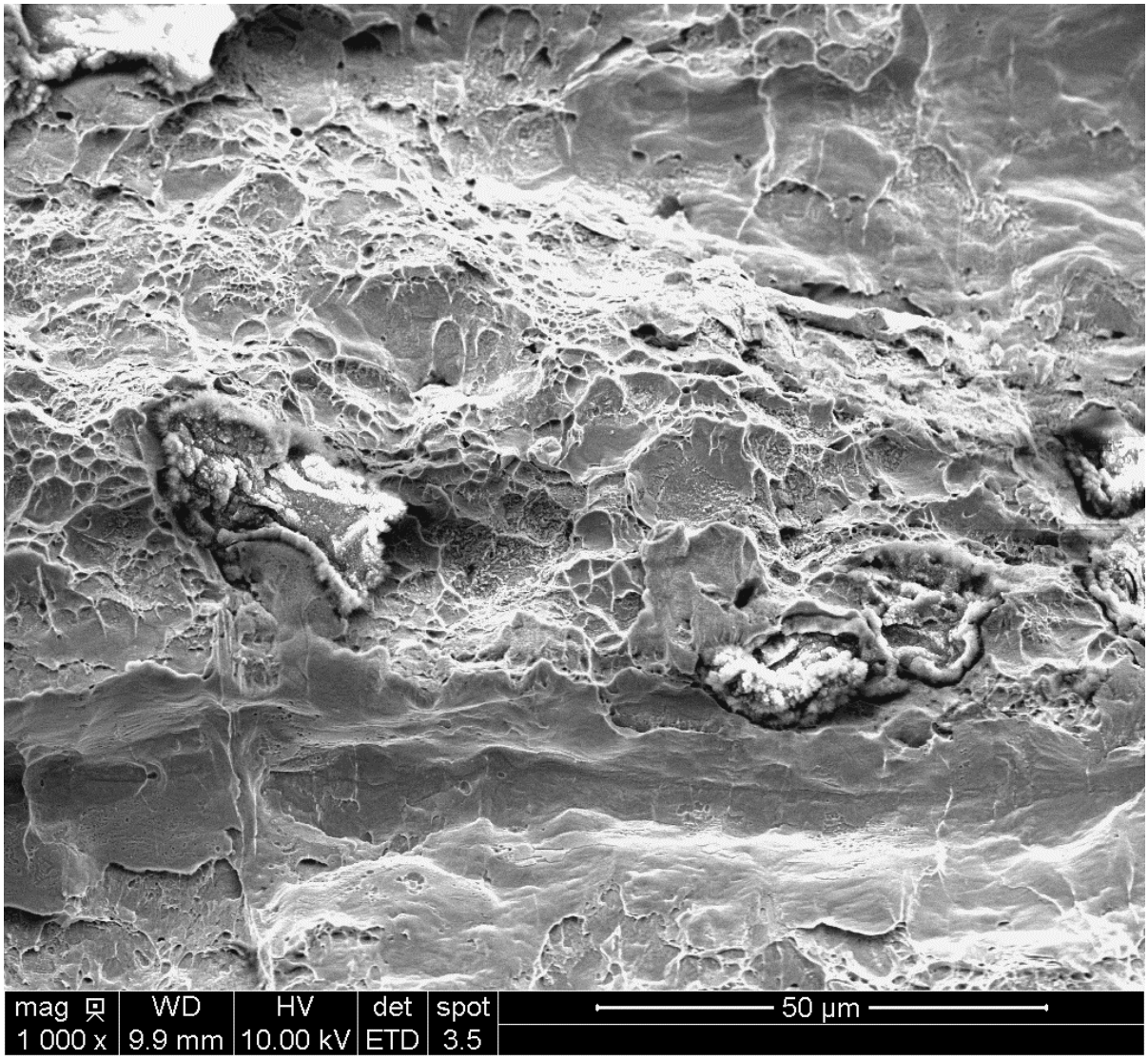

Figure 4-14. SEM Image of Ductile Rupture Just Beyond the Fatigue Crack at Location 6 in Figure 4-6

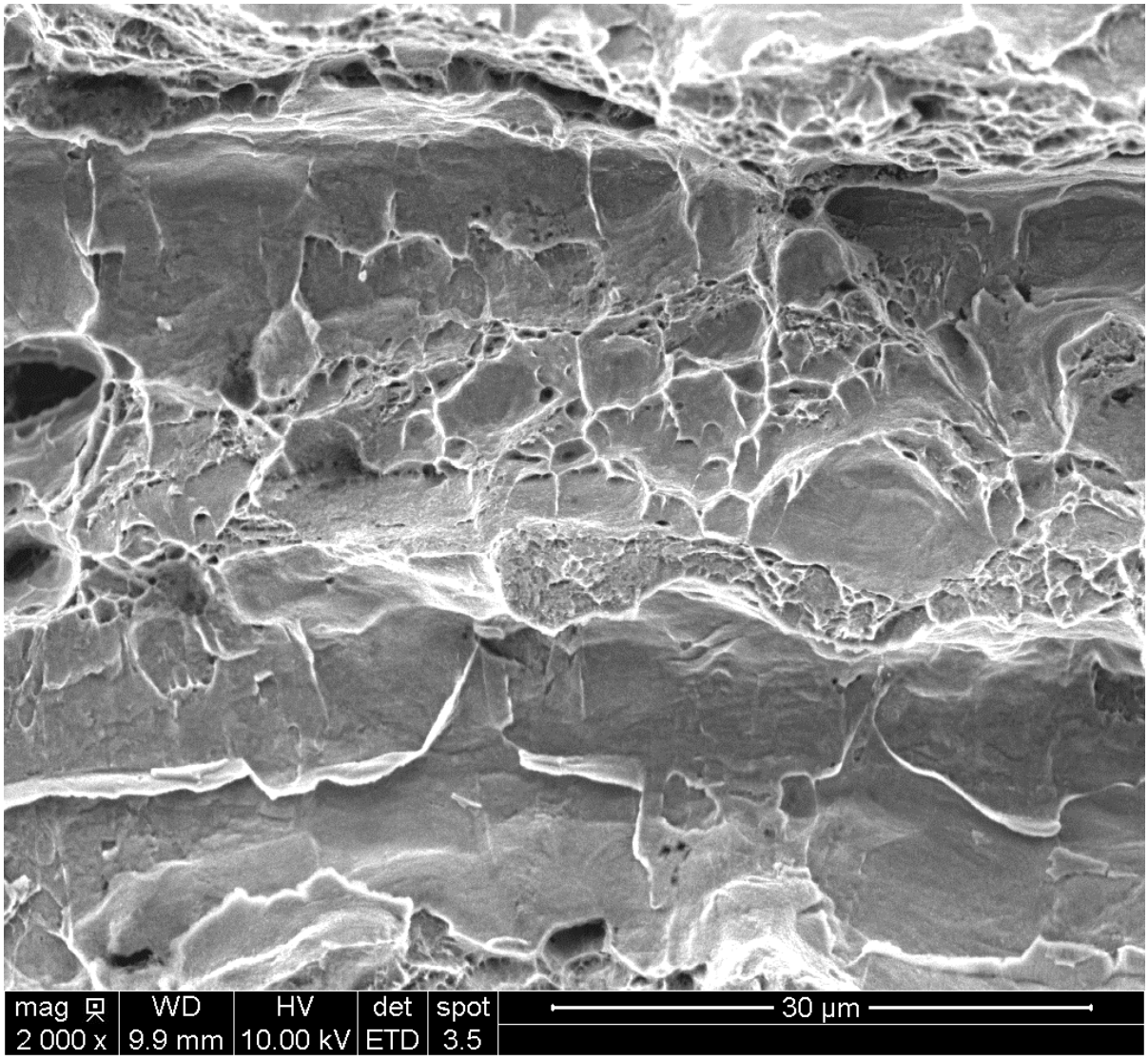

Figure 4-15. SEM Image of Ductile Fracture Features Within the Overload Region at Location 7 in Figure 4-6

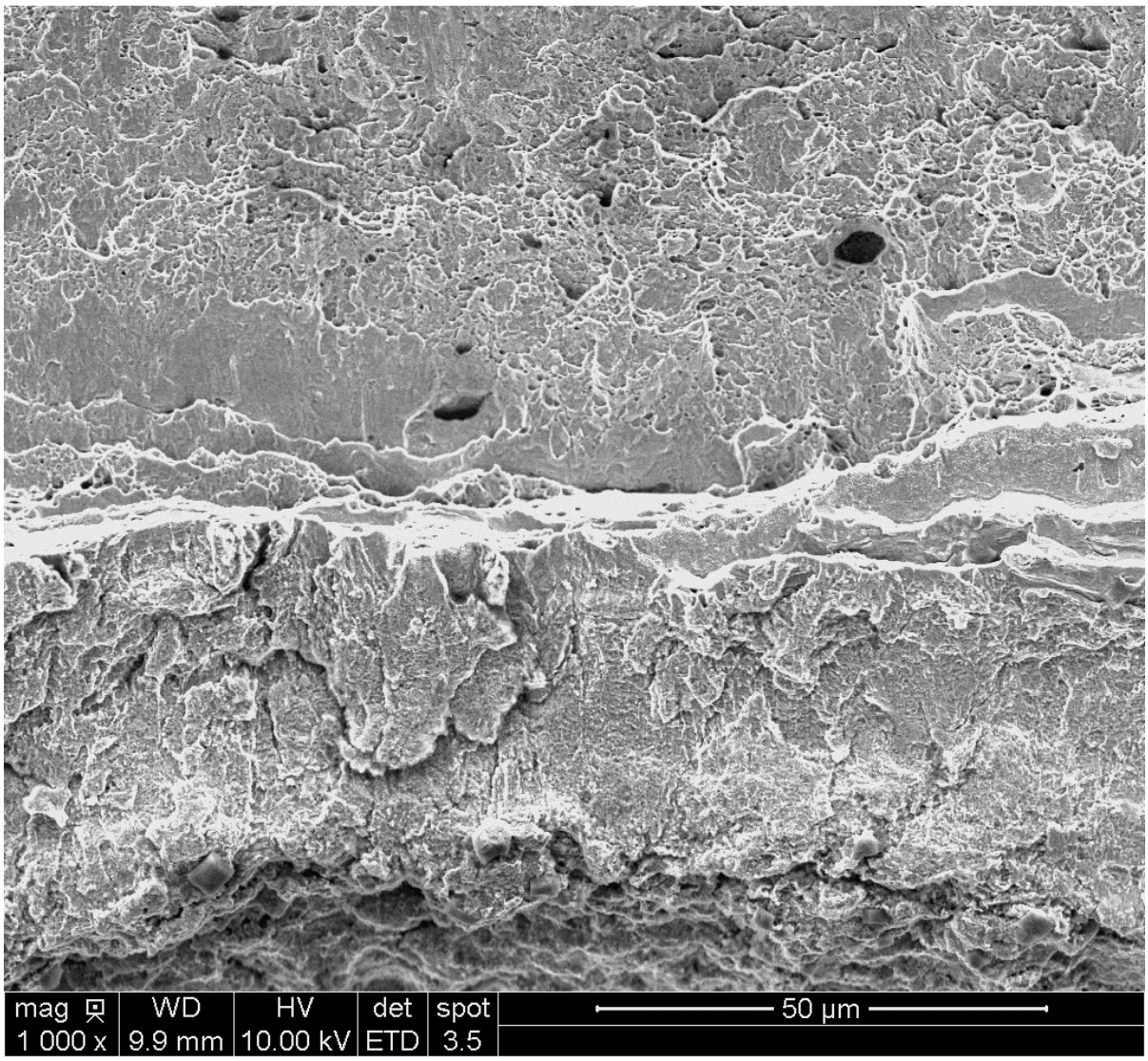

Figure 4-16. SEM Image of Ductile Features Along the I.D. Edge of the Fracture at Location 8 in Figure 4-6

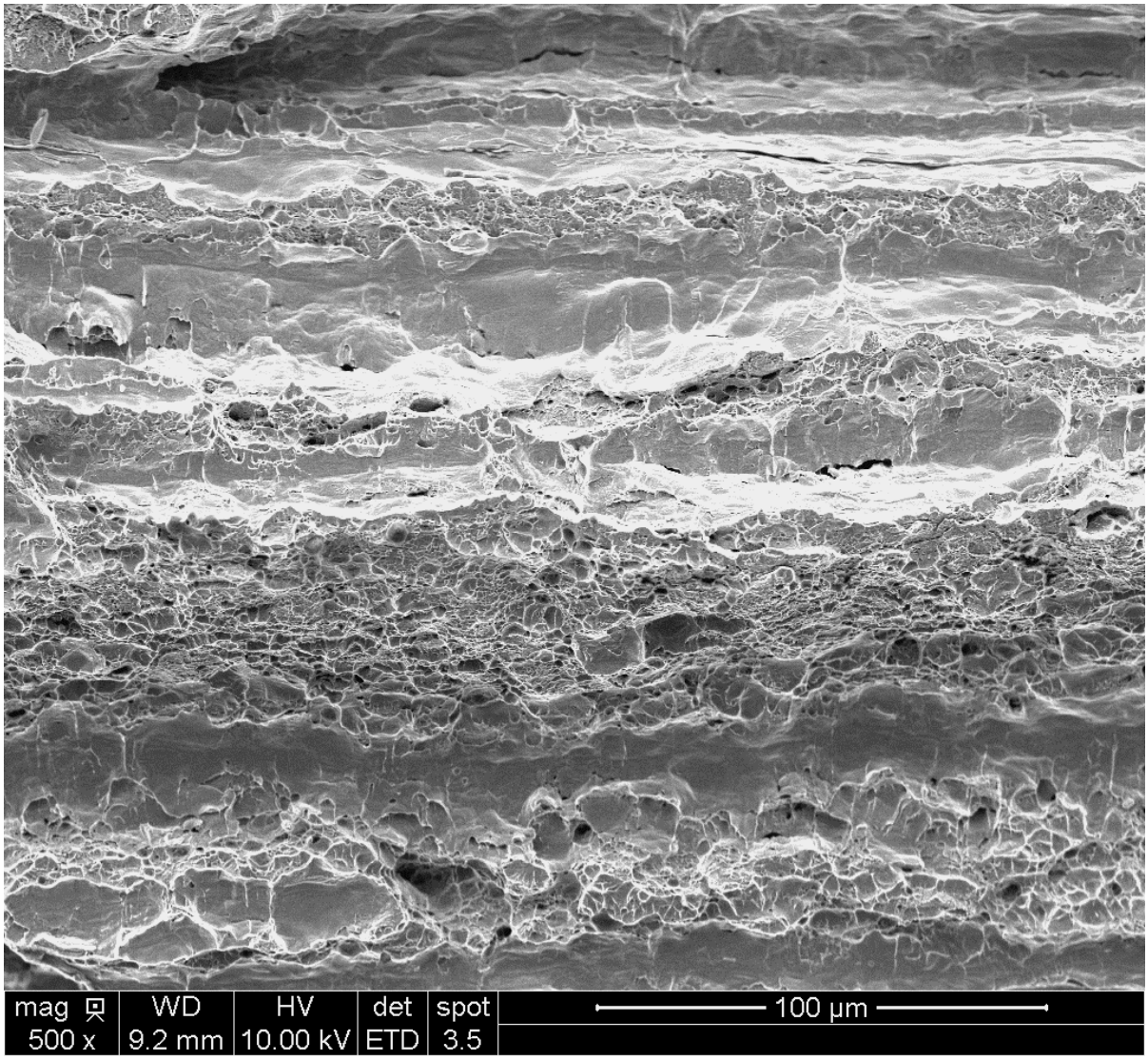

Figure 4-17. SEM Image of Ductile Fracture Features Within the Overload Region at Location 9 in Figure 4-6

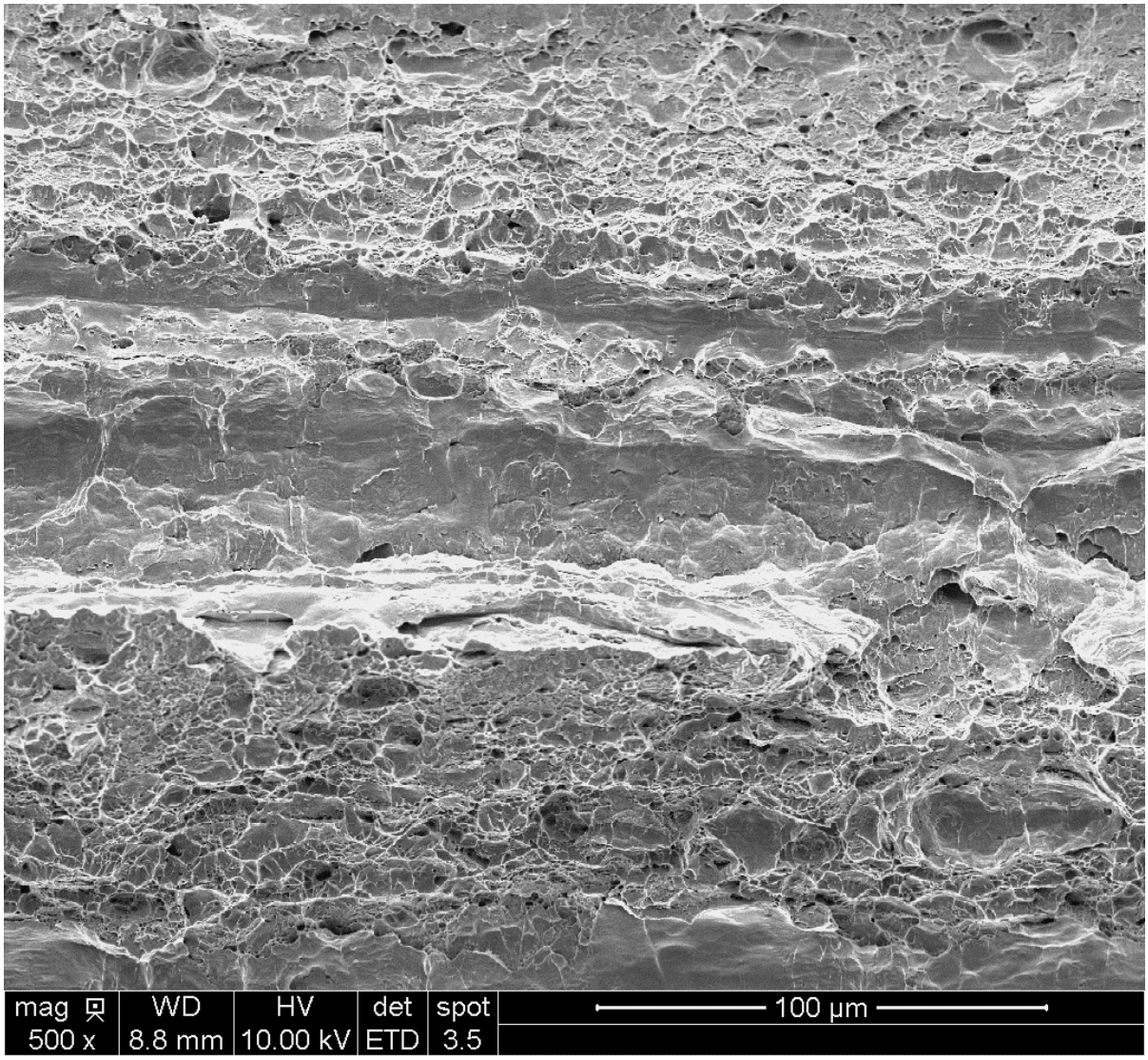

Figure 4-18. SEM Image of the Ductile Fracture Features Present in the Laboratory Fracture Region

5.0 MECHANICAL CHARACTERIZATION

Some basic mechanical testing was performed in order to characterize the mechanical behavior of the AO Smith 1146a shell and A-225 Grade B head materials. This characterization is an initial portion of an overall characterization of the pressure vessel constituents, including the heads, inner and outer shells and the welds (shell seam welds and head-to-shell girth welds).

5.1 Tensile Testing

Tensile testing was performed in keeping with ASTM E8 [1][1] on the AO Smith 1146a outer shell and the A-225 Grade B head materials. Standard 0.5-in. round tensile bars were machined from the head material in the longitudinal direction[2] while flat dog bone specimen with a nominally 0.25-in. square cross-section were machined from the outer shell in the hoop orientation. All testing was performed at room temperature.

The results of the tensile testing are presented in Table 5-1 for the 1146a shell and A-225 head materials. By way of reference, the tensile properties are compared to data available in a NASA Tech Memo [2]. The tensile properties of the A-225 Grade B head material are in very good agreement with the reference data. The properties of the 1146a outer shell material are in reasonable agreement with the reference data, but demonstrate a slight increase in strength and a slight reduction in ductility. While the source of the reference material is unclear, this testing was performed on material extracted from an actual pressure vessel. The slight differences in shell properties may be the result of the forming process in creating the multilayered body of the vessel.

Table 5-1. AO Smith 1146a and A-225 Gr.B Tensile Properties

Material	ID	Temp (°	Yield (ksi)		UTS (ksi)		Ductility (%)		Area Redu (%)
			Test	Ref [2]	Test	Ref [2]	Test	Ref [2]	
1146a ou shell	1	RT	86.1	75.0	118.7	101.3	23.0	31	41.0
	2		79.3		119.4		24.0		41.6
	3		81.3		119.2		23.0		43.6
	Ave		82.2		119.1		23.3		42.1
A-225 Gr. head	1	RT	53.1	58.4	80.0	82.1	34.0	34	67.2
	2		51.7		77.5		36.0		68.4
	3		52.7		80.4		33.0		67.8
	Ave		52.5		79.3		34.3		67.8

[1] Numbers in square brackets [#] refer to references listed in Section 8.

[2] All orientations are with respect to the pressure vessel geometry and not necessarily material directions.

5.2 Charpy V-Notch Testing

Charpy V-notch (CVN) testing was performed in keeping with ASTM E23 [3] on the AO Smith 1146a outer shell and the A-225 Grade B head materials. CVN testing was performed at room temperature and -20 ^{o}F. The limited thickness (nominally 0.25 in.) of the outer shell required the use of sub-sized CVN specimens in the C-L orientation[3]. These specimens had a 2-mm notch in a 10-mm width but were only 5 mm thick instead of the standard 10-mm thickness. Standard, full-sized specimens of 10-mm by 10-mm were used for the head material in the L-C orientation.

Both materials indicate a significant drop in CVN and lateral expansion from RT to -20 ^{o}F. Although this testing was not designed to determine the ductile-to-brittle transition temperature, these data are consistent with the reported nil-ductility temperature of -25 ^{o}F for the A-225 material and the reported decrease in CVN with temperature between RT and -20 ^{o}F for both A-225 and 1146a materials (nil-ductility for 1146a was not reported) [2].

The results of the Charpy testing are presented in Table 5-2 for the 1146a shell and A-225 head materials. A scaling factor [4, 5] was used to adjust the sub-size CVN data in order to facilitate comparison to available CVN values from standard 10-mm x 10-mm specimens. This scaling applies to sub-sized specimens of reduced thickness by simply scaling the measured sub-sized CVN energy by the ratio of the thickness reduction to the standard 10-mm thickness.[4] However, the thinner specimens have reduced notch-tip constraint, which can result in increased CVN energy. As the correction does not account for changes in notch-tip constraint, the thickness-corrected CVN energy may be an overestimation.

The scaled data is compared to data available in a NASA Tech Memo [2] in Table 5-2. The CVN energies are well below reported values [2]. Representative CVN specimens of the shell and head materials are shown in Figures 5-1 and 5-2, respectively. The fracture surface for both materials at room temperature and -20 ^{o}F is indicative of brittle failure. Some shear deformation associated with the formation of shear lips is evident at room temperature while negligible shear was noted at -20 ^{o}F. These fracture surfaces are indicative of the measured CVN energies. The source of the discrepancy with the reported values is currently unknown. It is unknown if these differences are attributable to the chemistry differences noted in Section 3.0.

---

[3] The first direction corresponds to the loading direction and the second indicates the crack growth direction.

[4]The ASME B&PV Code (Section VIII, Div. 3, Article KM-2) allows the use of subsize CVN specimens when material size or shape precludes the use of full-size CVN specimens and recommends scaling the results as done here.

Table 5-2. AO Smith 1146a and A-225 Gr. B CVN Properties

Material	Temp (^oF)	Test	Lateral Expansion (%)	CVN (ft-lbs)		
				Sub-Size[1]	Full-Size	Ref [2]
1146a ou shell	RT	1	6.1	7	14[2]	79
		2	9.9	7	14[2]	
		3	7.6	8	16[2]	
		Ave	7.8	7	15[2]	
	-20	1	2.3	4	8[2]	41
		2	2.8	3	6[2]	
		3	2.3	3	6[2]	
		Ave	2.5	3	7[2]	
A-225 Gr. head	RT	1	6.6		24	41
		2	5.8		20	
		3	5.8		19	
		Ave	6.1		21	
	-20	1	1.6		6	20
		2	1.5		6	
		3	1.4		5	
		Ave	1.5		6	

Notes: (1) sub-sized specimens of 10x5x2V

(2) CVN adjusted to standard 10x10x2V per [4, 5]

(a) RT ..... (b) -20 ^{o}F

Figure 5-1. AO Smith 1146a Shell CVN Specimens

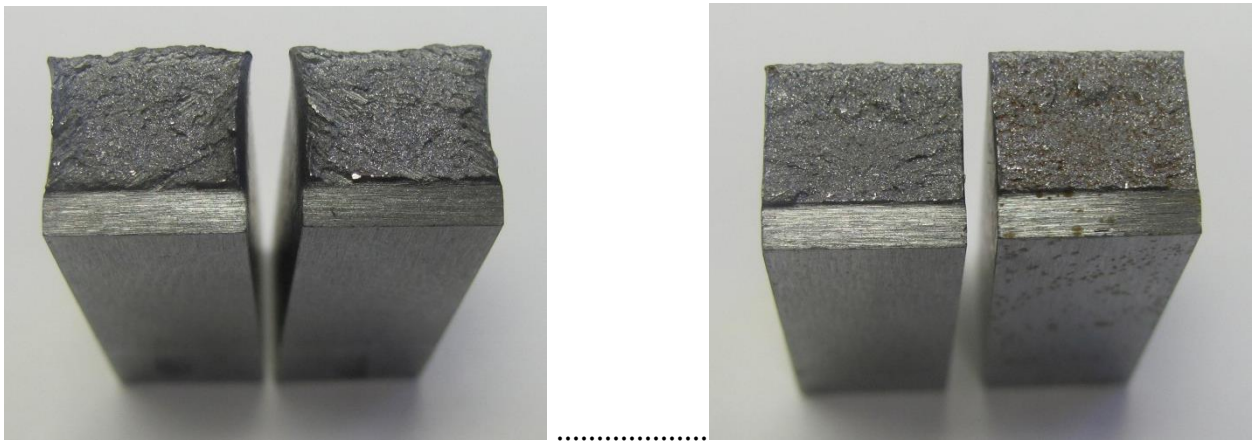

(a) RT ..... (b) -20 ^{o}F

Figure 5-2. A-225 Head CVN Specimens

5.3 Plane Strain Fracture Toughness – A-225 Grade B Head Material

Plane strain fracture toughness testing was performed in keeping with ASTM E399 [6] for the A-225 Grade B head material – plane strain toughness testing was believed to be unsuitable for the 1146a shell material given its limited thickness. Testing was performed using compact tension, C(T), specimens with a width, W, of 2 in. and thickness, B, of 1 in. (see Figure 5-3). The test set-up showing the specimen, clip gage and traveling microscope (behind) is shown in Figure 5-4.

Prior to toughness testing, specimens were polished to a mirror-like finish to aid in visually measuring the crack length during precracking. Crack length was measured on both sides of the specimen using traveling microscopes with digital verniers. The load during precracking was kept in the range of 60-80 percent of the anticipated fracture load in accordance with ASTM E399.

Unfortunately, with the low yield and apparently high toughness of the A-225 head material, significant plasticity and severe blunting of the crack tip developed during testing. A typical

specimen following testing is shown in Figure 5-5 that indicates the extreme plasticity at the crack tip and considerable lateral contraction through the thickness. The results so grossly violate the conditions of ASTM E399 for plane strain toughness that subsequent data analysis was not performed.

Based on the yield and apparent toughness of the A-225 material, a C(T) with an estimated W of 12 in. would be required in order to achieve a valid plane strain toughness measure. Similarly, an estimated W of 9 in. would be required to obtain a plane stress toughness measure per an ASTM E561 K-R approach [7]. Thus, it is recommended that toughness testing of the A-225 head material be performed in keeping with the J-R approach of ASTM E1820 [8].

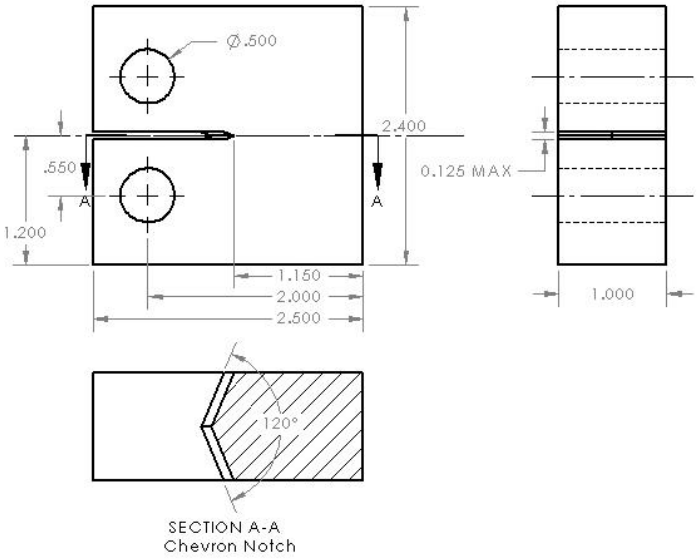

Figure 5-3. Plane Strain Fracture Toughness Specimen Drawing

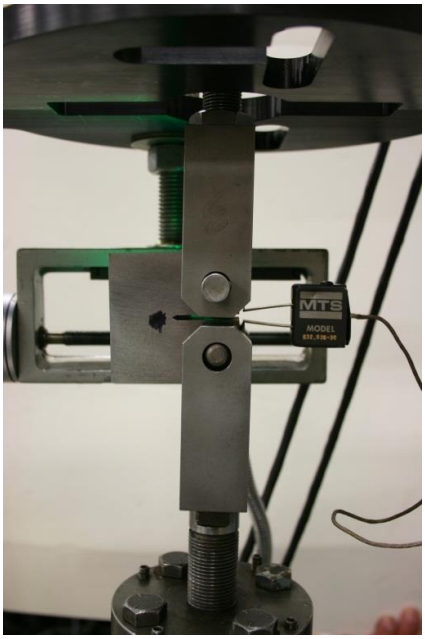

Figure 5-4. Plane Strain Fracture Toughness Test Set-up

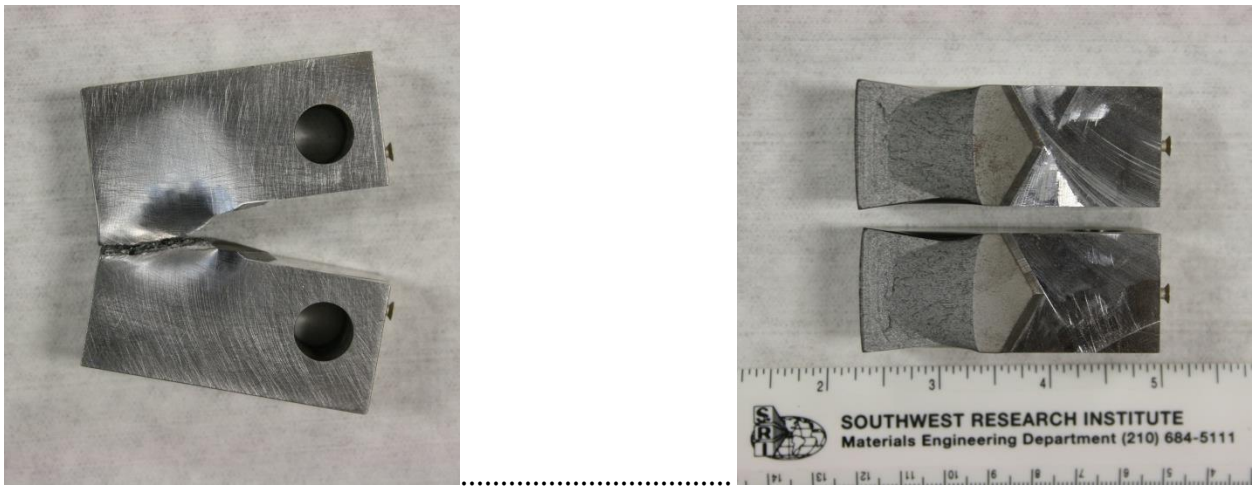

Figure 5-5. Typical A-225 Specimen After Toughness Testing

5.4 Plane Stress Fracture Toughness Testing – AO Smith 1146a Shell Material

Given the limited thickness of the outer shell material, determining a valid plane strain toughness was deemed unlikely. Thus, a K-R approach per ASTM E561 [7] was used to determine the plane stress toughness. C(T) specimens with W=1.25 in. and B= 0.24 in. were extracted from the shell in the C-L orientation such that the specimen would be loaded in the hoop direction and a crack in the axial direction (see Figure 5-6).

Following precracking, the specimen was loaded to failure while measuring crack extension. For the room temperature testing, crack extension was measured visually using traveling microscopes with digital verniers. For the -20 ^{o}F testing in which visual measurements were not possible, crack extension was measured using a standard direct current potential drop (DCPD) technique in which the specimen is subjected to a constant current and the measured voltage potential drop across the crack is related to crack length. This set-up, without the cold chamber, is shown in Figure 5-7 and includes the DCPD wires attached to the specimen.

The resulting crack growth resistance, K_R, is plotted as a function of crack extension and overlaid with crack driving force, K, curves of constant load (refer to Figure 5-8). The load (P_3 in Figure 5-8) associated with the curve tangent to the K_R curve is the critical load at instability and is used to establish the plane stress toughness, K_c, for the material for its tested thickness.

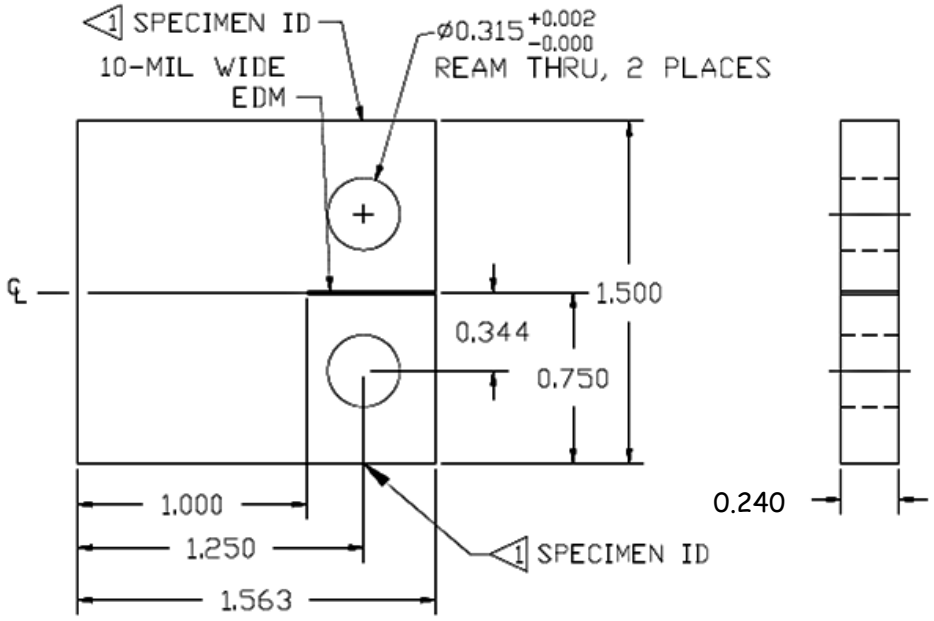

Figure 5-6. Plane Stress Fracture Toughness Specimen Drawing

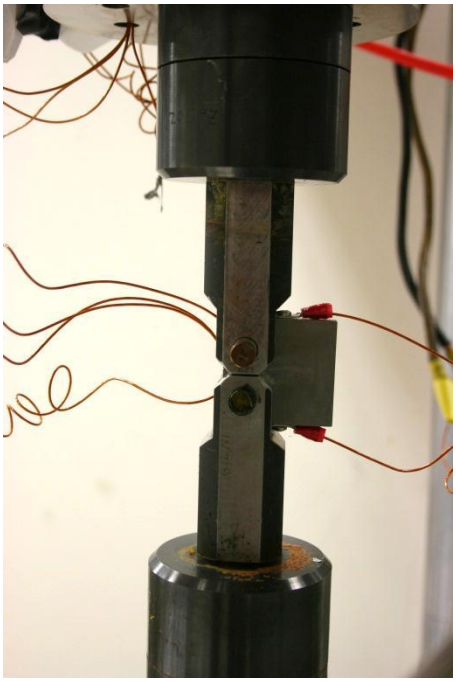

Figure 5-7. Plane Stress Fracture Toughness Test Set-up

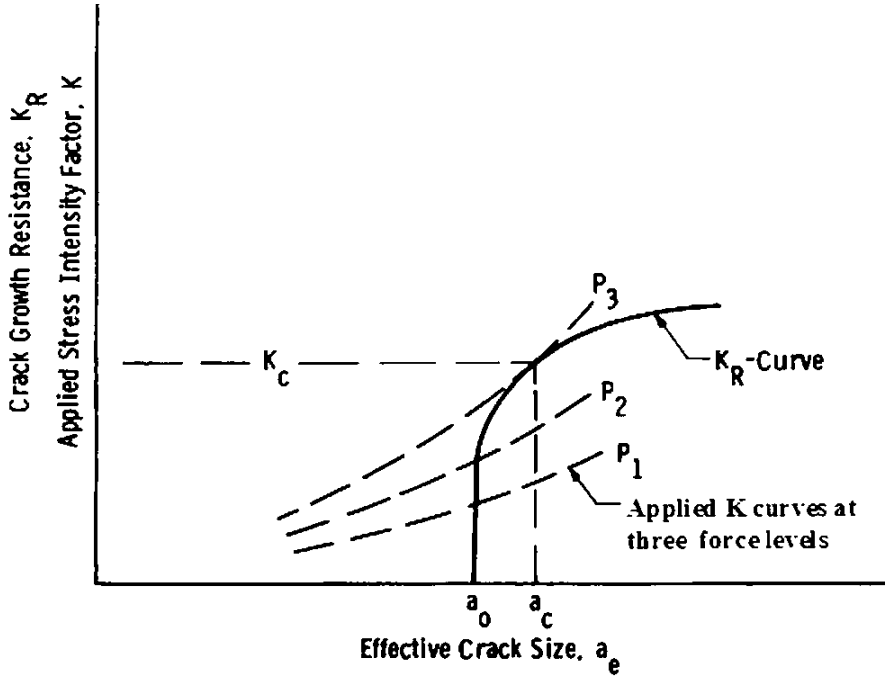

Figure 5-8. Schematic of the K-R Approach Used in Determing K_c (Ref [6])

This approach was used to establish the plane stress fracture toughness for the AO Smith 1146a outer shell material (see Table 5-3). As noted in Table 5-3, the initial crack lengths of two room temperature tests were ultimately found to be slightly out of specification per ASTM E561. However, a re-test with an initial crack length within specification resulted in very consistent toughness, suggesting that those values are reasonable. These toughness values are also

consistent with a reported toughness of 82 ksi√in for a comparable sized specimen [2]. Little difference in toughness was noted between RT and -20 °F, which is consistent with the general findings in [2].

Table 5-3. AO Smith 1146a Shell Plane Stress Fracture Toughness

Material	Temp (°F)	B (in)	W (in)	a_o (in)	K_c ksi√in
1146a outer sh	RT	0.236	1.249	0.3505*	92
		0.236	1.248	0.3465*	91
		0.237	1.249	0.4440	88
		---	---	Ave	90
	-20	0.236	1.250	0.4310	86
		0.237	1.249	0.4870	86
		---	---	Ave	86

Note: * crack length required to be 0.391 and 0.625 in.

5.5 Fatigue Crack Growth Behavior

Fatigue crack growth (FCG) testing was performed in keeping with ASTM E647 [9] on the AO Smith 1146a outer shell and the A-225 Grade B head materials using standard C(T) specimens (see Figures 5-6 and 5-9, respectively, for the 1146a and A-225 materials). Note that a smaller specimen was used for the 1146a shell material due to limitations in thickness and curvature.

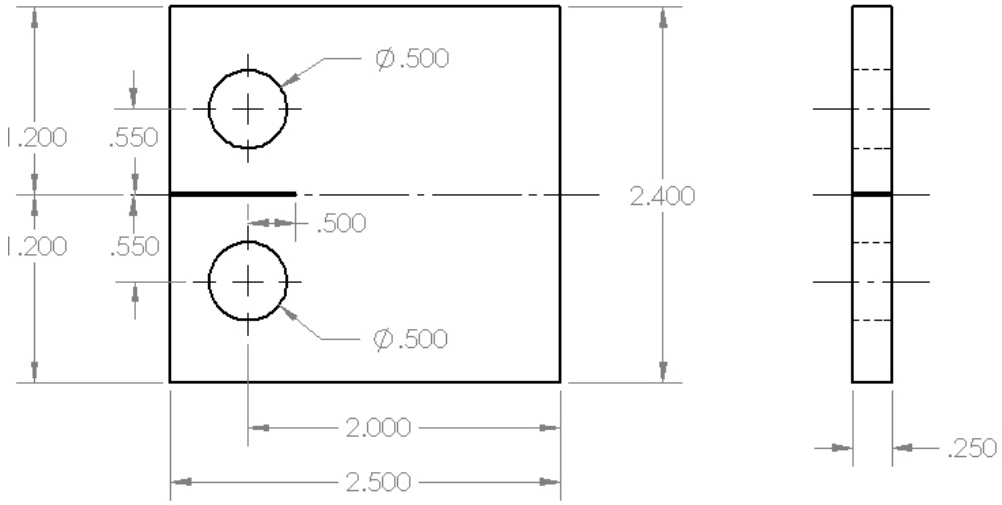

Figure 5-9. FCG Specimen Drawing for the A-225 Gr B Material

Testing was performed on a 50-kip servohydraulic test frame equipped with an MTS 458.20 controller and Fracture Technology Associates (FTA) software specifically designed for ASTM E647 FCG testing. Prior to FCG testing, specimens were polished to a mirror-like finish to aid in visually measuring the crack length. Digital vernier traveling microscopes were used to visually measure crack length on front and back faces. The test set-up is shown in Figure 5-10.

A standard direct current potential drop (DCPD) technique was used to infer the instantaneous crack length during FCG testing. The corresponding Johnson's equation coefficients were used with the FTA system to determine the crack length as described in ASTM E647 [9]. Typically three to five visual measurements were performed throughout the FCG test and used in post-test corrections of the DCPD-inferred crack lengths in keeping with ASTM E647.

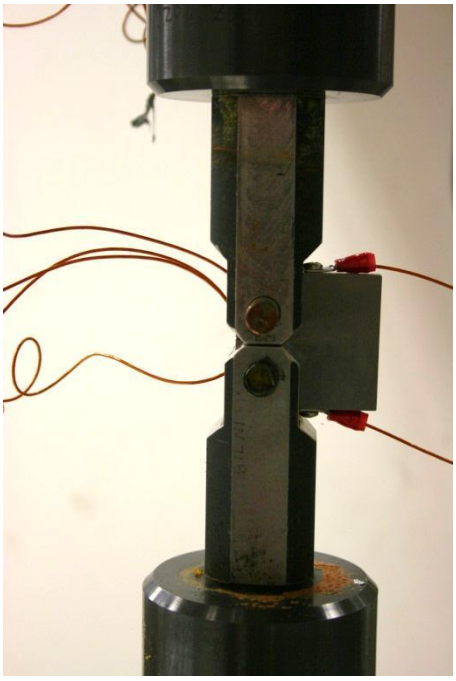

Figure 5-10. FCG Test Set-Up (1146a Specimen Shown)

Specimen pre-cracking was performed per ASTM E647. Pre-cracking conditions were designed to mitigate any load history effects that might compromise subsequent FCG test results. At the end of pre-cracking, the final pre-crack length was measured on both the front and back faces of the specimen.

All FCG testing was performed at a load ratio, R, (ratio of minimum to maximum load) of 0.15 and at RT. Constant amplitude FCG testing was utilized to establish the fatigue crack growth rate behavior above a growth rate of nominally 4×10^{-7} in/cyc. As testing progresses under constant amplitude, ΔK increases as the crack length increases. This constant amplitude strategy was used to characterize the majority of the FCG behavior.

In order to characterize the near-threshold behavior, a K-decreasing method was utilized. This method uses the instantaneous crack length determined from DCPD to adjust the applied cyclic loading and gradually load-shed to ultimately approach threshold behavior, ΔK_{th}. For this testing, a gradient, C, of -2 $in.^{-1}$ was used and is the maximum shedding rate allowed by ASTM E647. Also per ASTM E647, K-decreasing testing was restricted to starting below a growth rate of $4x10^{-7}$ in/cyc. K-decreasing testing was allowed to continue to growth rates in the 10^{-9} in/cyc decade where data indicated threshold behavior after which continued testing was performed under constant amplitude (increasing ΔK) until test completion.

Upon completion of each fatigue crack growth test, the data generated was post-processed to calibrate the DCPD crack length measurements with the visual crack lengths that were recorded periodically during the entire test. This procedure was performed using the FTA Automated Fatigue Crack Growth Analysis software (2001 series, version 3.05.03a, FTA).

The resulting da/dN-ΔK FCG behavior for the 1146a and A-225 materials is shown in Figures 5-11 and 5-12, respectively. The results are typical of FCG behavior, characterized by a near threshold region of little/no crack growth followed by a so-called Paris region where growth rate is proportional (on log-log scale) to cyclic driving force. At driving forces approaching material toughness, the growth rate accelerates to failure. Loss of validity of the test data occurred in this region as the crack was especially deep and close to the back face of the specimen, violating LEFM considerations. These data are represented by open symbols throughout this report. It may be appropriate to develop additional data in the near-threshold and near-failure regions during the second phase of this program.

It is important to note that the FCG data generated for each material consists of two individual tests. The inability to discern these individual tests is an indication of the repeatability of the data generated.

Also included in Figures 5-11 and 5-12 are FCG data generated by NASA Langley (LaRC) [2]. The Langley data were generated with R = 0.05 (recall that data generated in this SwRI effort were at R = 0.15). While the Langley data certainly has considerable scatter, there appears to be reasonable consistency given the difference in R between these data sets since one would expect the R = 0.15 data to be only slightly higher than the R = 0.05 data. The new data obtained herein lie above the Langley data for both materials.

A comparison of the 1146a and A-225 FCG behavior is shown in Figure 5-13. The behavior of the two materials is extremely consistent, including the near threshold region.

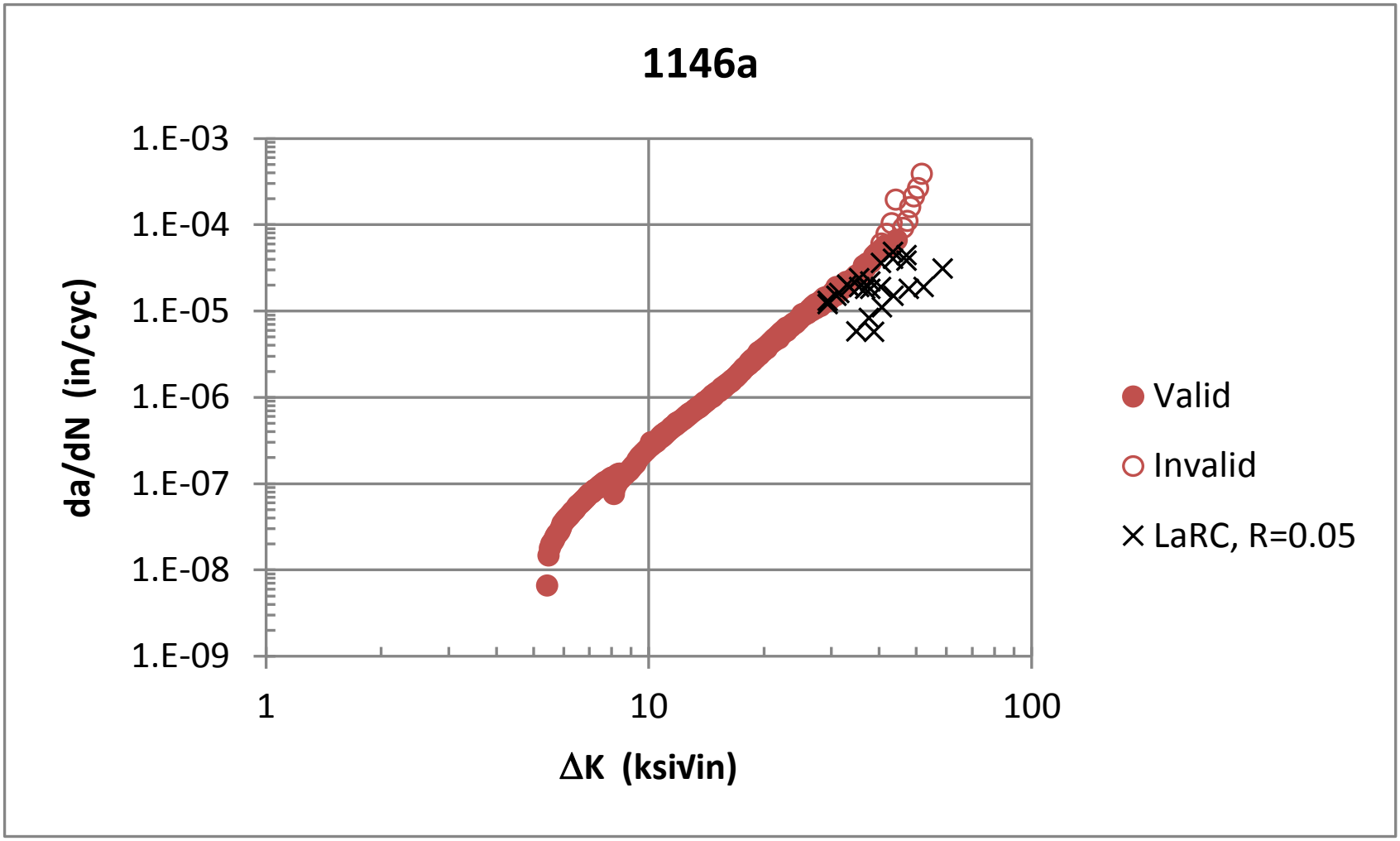

Figure 5-11. AO Smith 1146a Outer Shell FCG Behavior at R = 0.15

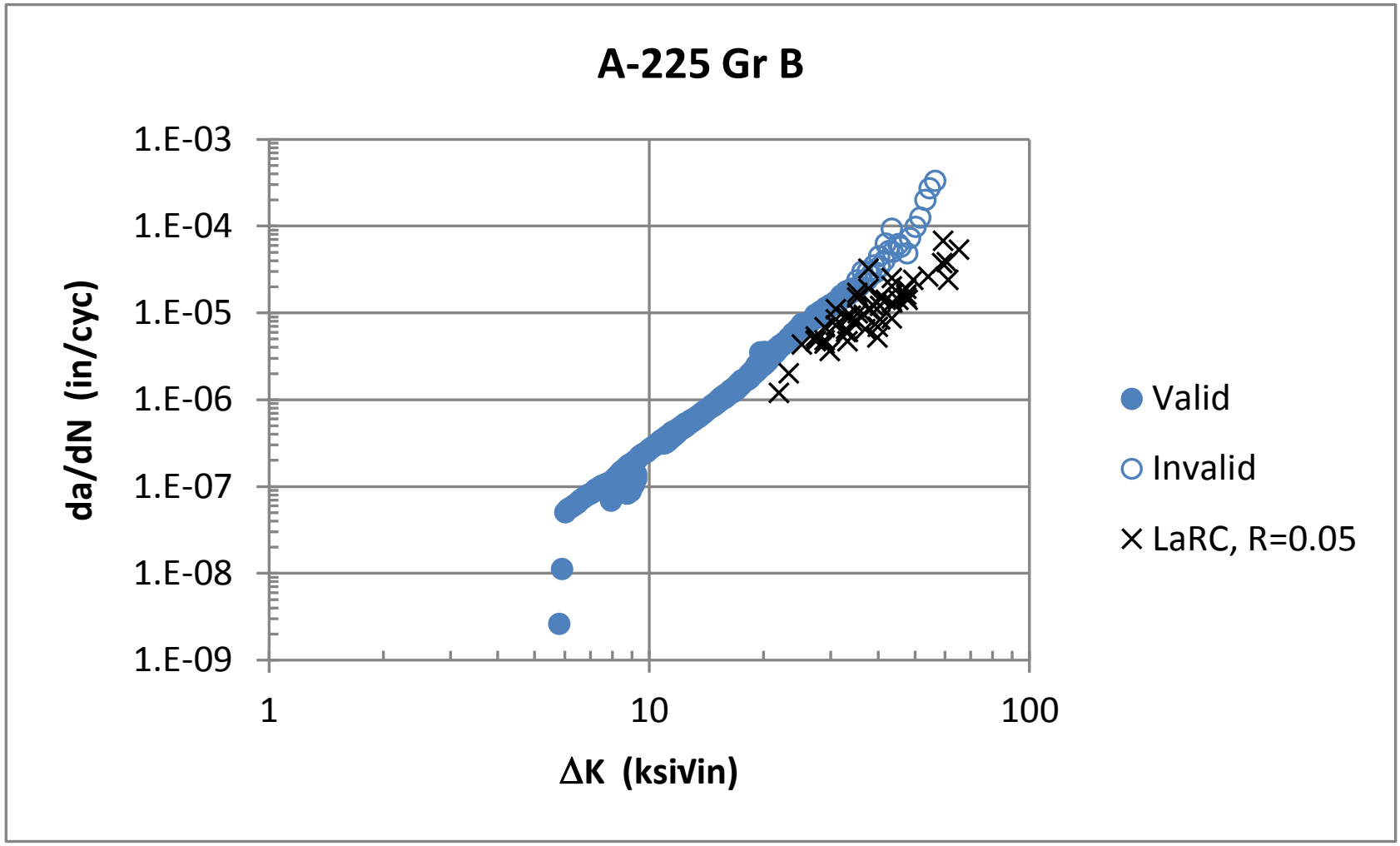

Figure 5-12. AO Smith 1146a and A-225 Gr. B FCG Behavior at R = 0.15

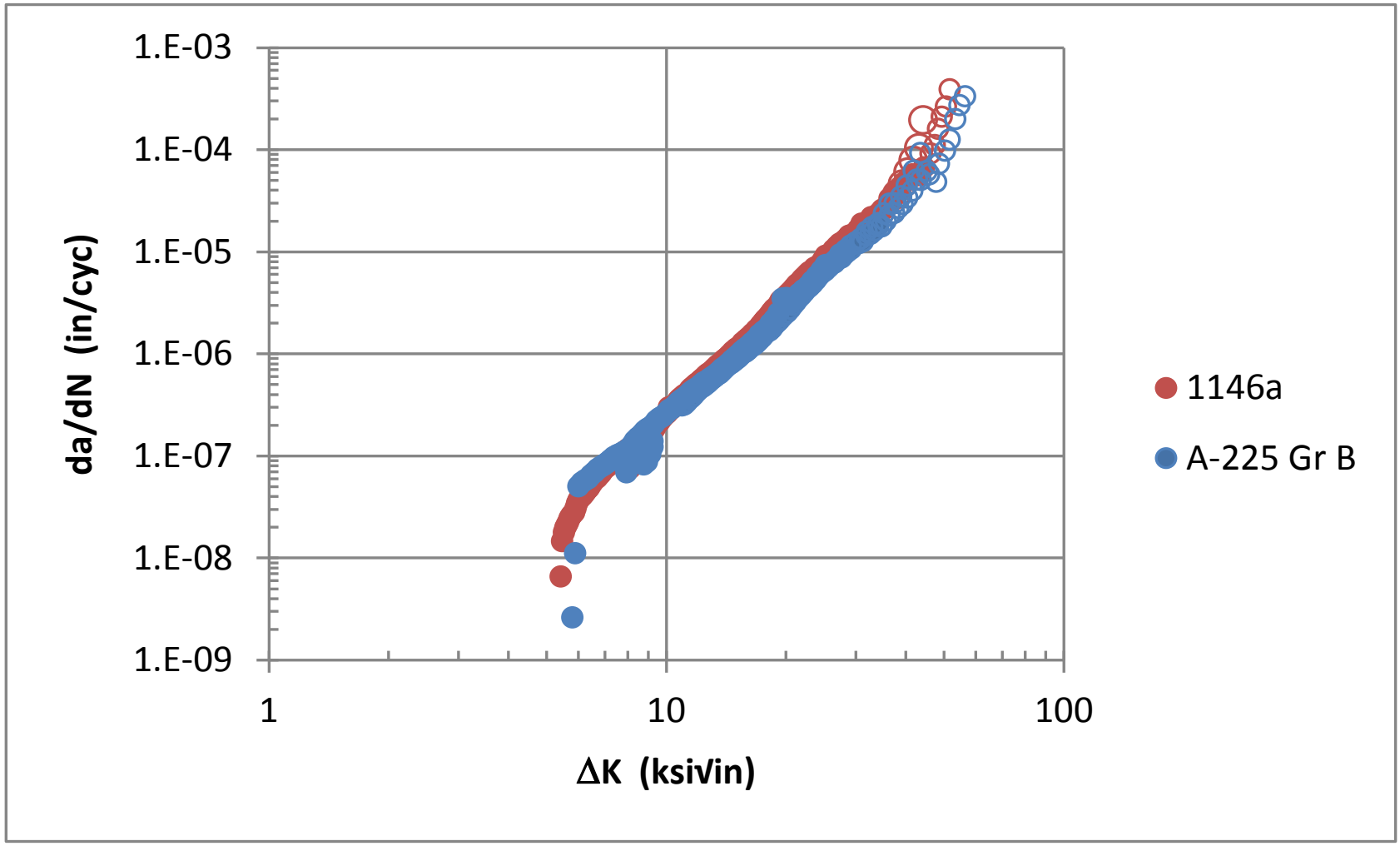

Figure 5-13. Comparison of 1146a and A-225 FCG Behavior at R = 0.15

5.6 Mechanical Characterization Summary

Tensile, Charpy V-notch, fracture toughness and fatigue crack growth testing was performed on the AO Smith 1146a outer shell and A-225 Grade B head materials. The following provides a summary of the findings.

- The tensile properties of both materials were in reasonable agreement with reference tensile data [2]. A slight increase in strength and a slight reduction in ductility with respect to the reference data were noted for the 1146a material. These slight differences may be the result of forming process in creating the multilayered body of the vessel.
- The Charpy V-notch results of the A-225 head material and 1146a shell material, even when adjusted for sub-size specimens, were very low and much lower than the reference data. The source of this difference is unknown.
- Both materials indicate a significant drop in CVN from RT to -20 ^{o}F. This is consistent with the reported nil-ductility temperature of -25 ^{o}F for the A-225 material and the reported decrease in CVN with temperature between RT and -20 ^{o}F for both materials [2].
- Plane strain fracture toughness testing of the A-225 Grade B material resulted in grossly invalid conditions due to its high apparent toughness and low yield. The extreme ductility and plasticity at the crack tip would necessitate a J-R approach in order to obtain a valid toughness measure, which was not within the scope of this Phase 1 effort.
- The plane stress fracture toughness of the 1146a material, based on a K-R approach for a nominal 0.25-in. thickness, was consistent with the reported toughness of similar thickness. Little difference was noted between RT and -20 ^{o}F, consistent with the general findings in [2].
- The fatigue crack growth behavior at R = 0.15 was developed for both materials at RT. The FCG behavior includes the general Paris region as well as some near-threshold behavior. Loss of validity limited the behavior at upper regions of the da/dN-ΔK behavior.
- The FCG behavior of the 1146a and A-225 materials was indistinguishable.

5.7 Considerations for Phase 2 Characterization Testing

The testing reported herein consisted of an initial portion of an overall characterization of the pressure vessel constituents, including the heads, inner and outer shells and the welds (shell seam welds and head-to-shell girth welds). Based on the results and findings of this effort, the following are considerations for the scope of the follow-on Phase 2 characterization.

- As the intent was to characterize both the RT and -20 ^{o}F behavior of all of the pressure vessel constituents, a limited amount of tensile testing should be performed at -20 ^{o}F. This will not only elucidate the low-temperature tensile properties, but also facilitate more robust low-temperature toughness and FCG characterization, which is a function of material yield.
- The Charpy results of the 1146a material were surprisingly low and significantly lower than reference values. This testing should be revisited to ensure confidence in the results.
- Given the high apparent toughness and low yield strength of the A-225 head material, a J-R approach should be considered to determine the toughness of the head material.
- Some additional, targeted FCG testing should be performed to provide additional data in the near-threshold and near-failure regions for both materials.

- Although most steels exhibit very little R-ratio dependence, particularly in the Paris region, a limited amount of FCG at a distinctly different R (likely a very high R) should be considered to support more complete FCG characterization for use in fitting the NASGRO equation.
- Although toughness did not exhibit any significant temperature dependence (the 1146a material did not in this effort and reference data indicated that neither material exhibits much), the development of a limited amount of FCG at an existing R-ratio (0.15) should be considered in order to determine the influence of temperature on FCG behavior.

6.0 FRACTURE MECHANICS ANALYSIS OF FLAW IN OUTER SHELL

6.1 Stress Analysis

Using the nominal shell dimensions (OD = 36.25 inches and T = 3.125 inches) and the standard thick-walled cylinder solution, the stress distribution through the thickness of the vessel shell wall was computed for a unit (1.0 ksi) internal pressure and is shown in Figure 6-1 plotted as a function of normalized distance, x/T. The red lines in the figure represent the thickness of the outer layer of the shell (0.25 inches) and over this short thickness the hoop stress is nearly linear decreasing from 4.408 ksi on the inside of the outer layer to 4.347 ksi on the outer surface. This stress gradient (in the outer layer) was used in the fracture mechanics and fatigue crack growth analyses that follow.

6.2 Fracture Mechanics Analysis

The notch and fatigue crack surface was shown in Figure 4-1 and, as previously mentioned, the fatigue crack did not grow laterally along the outer surface of the shell. The total notch length was 2.01 inches and for the purposes of analysis is set equal to 2c where c is the half-crack/notch length along the surface (c = 1.0 inches). The initial depth of the notch, a, was 0.172 inches and the fractographic analysis showed that it grew by fatigue 0.06 inches to a total depth of 0.232 inches. A 0.03 inch ligament was present between the tip of the fatigue crack and the inner surface of the plate that failed rapidly according to the fractographic analysis. The thickness, t, of the shell outer layer at the location of the notch was measured to be 0.26 inches (as compared to the nominal specified shell thickness of 0.25 inches).

It is unusual that the fatigue crack grew primarily in the through-thickness (depth) direction. That is, the crack length, 2c, remained essentially constant at about 2.0 inches while the crack grew only in the depth direction. It is suspected that the machining process used to "insert" the notch into the surface of the outer shell induced compressive residual stresses at the point where notch intersected the surface and that precluded fatigue crack growth from the surface crack tips. However, this is merely a logical explanation and it cannot at present be verified.

The NASGRO [10] surface crack in a plate model SC02 was used to perform the fracture mechanics and fatigue crack growth analysis of the flaw in the outer layer of the shell using the outer layer thickness of 0.26 inches. This model is a univariant weight function model capable of handling a nonlinear through-thickness stress gradient as shown in Figure 6-2. The stress gradient is that shown in Figure 6-1 between the red lines for the outer layer and is applied through-the-thickness. A width, W, of 24 inches was assumed. Note that this model neglects any effect of the curvature of the shell which is minimal at the large diameter to thickness ratio of the outer shell.

Normalizing the stress gradient allows the computation of geometry factors as a function of crack size and facilitates computing the stress intensity factor, K, for any internal pressure (or hoop stress). The geometry factors were computed using the NASSIF module of NASGRO and can be used to compute the stress intensity factor at any crack depth for this problem according to the following expression:

$$K(a) = p*(SF)*F(a)*\sqrt{\pi a} \quad (6.1)$$

where p is the internal pressure (ksi), SF is a scale factor (4.347) to convert the internal pressure to hoop stress in the outer layer, F(a) is the geometry factor for the crack depth, a, (the a-tip). K(a) is the stress intensity factor at the a-tip in units of ksi√in. Similarly, the stress intensity factor at the surface (the c-tip) is computed as:

$$K(c) = p*(SF)*F(c)*\sqrt{\pi a} \quad (6.2)$$

where F(c) is the geometry factor for the surface crack tip. Values of F(a) and F(c) are plotted in Figure 6-3 and tabulated in Table 6-1. Note that for this crack geometry, since the surface crack length never changed, the aspect ratio (defined as a/c) is equal to the crack depth since c is always 1.0 inches.

At the beginning of the cyclic pressure testing, the initial maximum pressure was 6.6 ksi and, therefore, the initial stress intensity factors at the a-tip and the c-tip can be computed as follows:

$$K(a=0.172) = 6.6(4.347)*1.612*\sqrt{\pi}(0.172) = 34.0 \text{ ksi}\sqrt{\text{in}}$$

$$K(c=1.0) = 6.6(4.347)*0.892*\sqrt{\pi}(0.172) = 18.8 \text{ ksi}\sqrt{\text{in}}$$

At the point of maximum fatigue crack depth (a = 0.23 inches) the geometry factor F(a) is 1.655. Near the end of the test (see the following section) the peak internal pressures were 10 ksi and 14 ksi. Repeating the above calculation for K(a=0.23) for these pressures gives stress intensity factors of 61.2 ksi√in for the 10 ksi peak pressure and 85.6 ksi√in for the 14 ksi peak pressure. Table 5-3 lists fracture toughness values obtained for the shell material (and thickness) that average 90 ksi√in at room temperature and 86 ksi√in at -20°F. Therefore, it can be concluded that the region of rapid fracture (spanning the 0.03 inch remaining ligament shown in Figures 4-1, 4-2 and 4-5) most likely occurred during one or more of the few 14 ksi pressure cycles near the very end of the test since the applied K was so close to the fracture toughness.

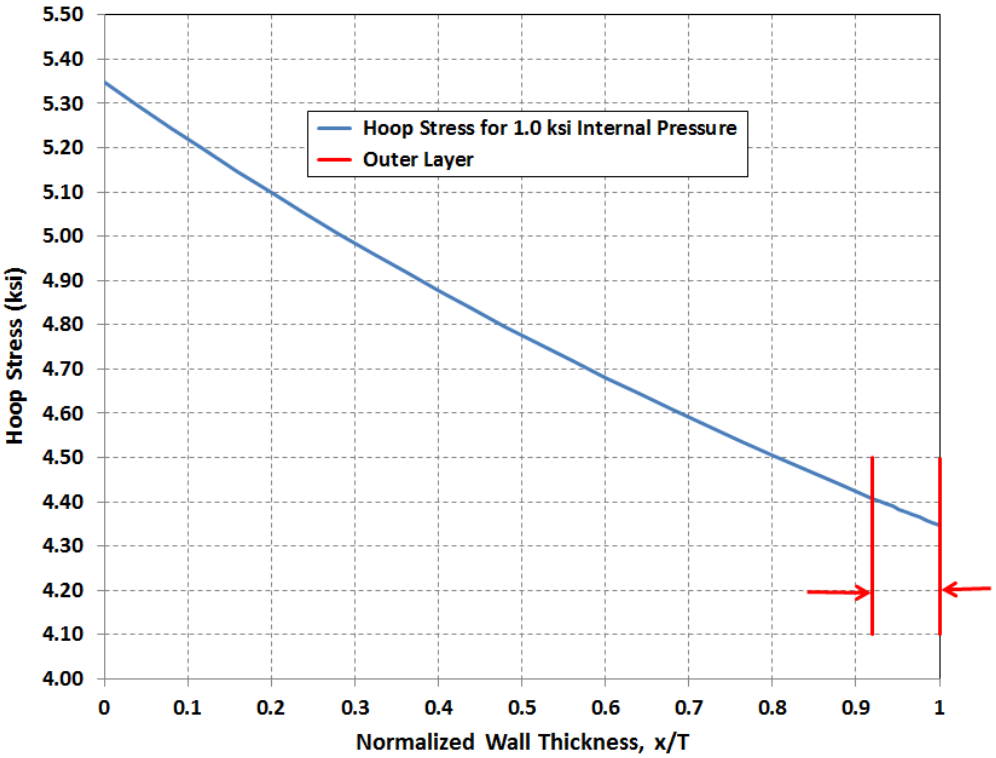

Figure 6-1. Hoop Stress Distribution in Shell Wall for a Unit Internal Pressure of 1.0 ksi

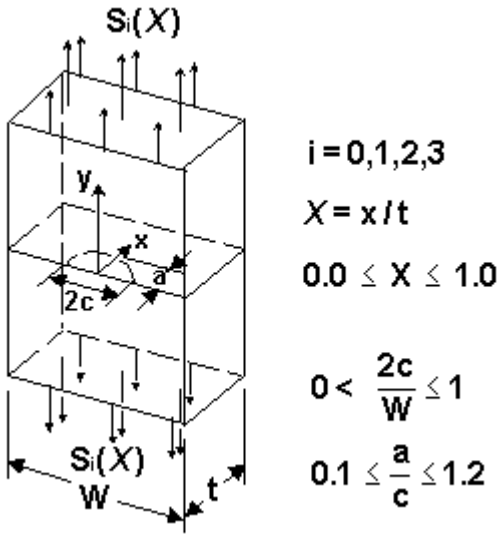

Figure 6-2. NASGRO Surface Crack in a Plate Fracture Mechanics Model SC02 [10]

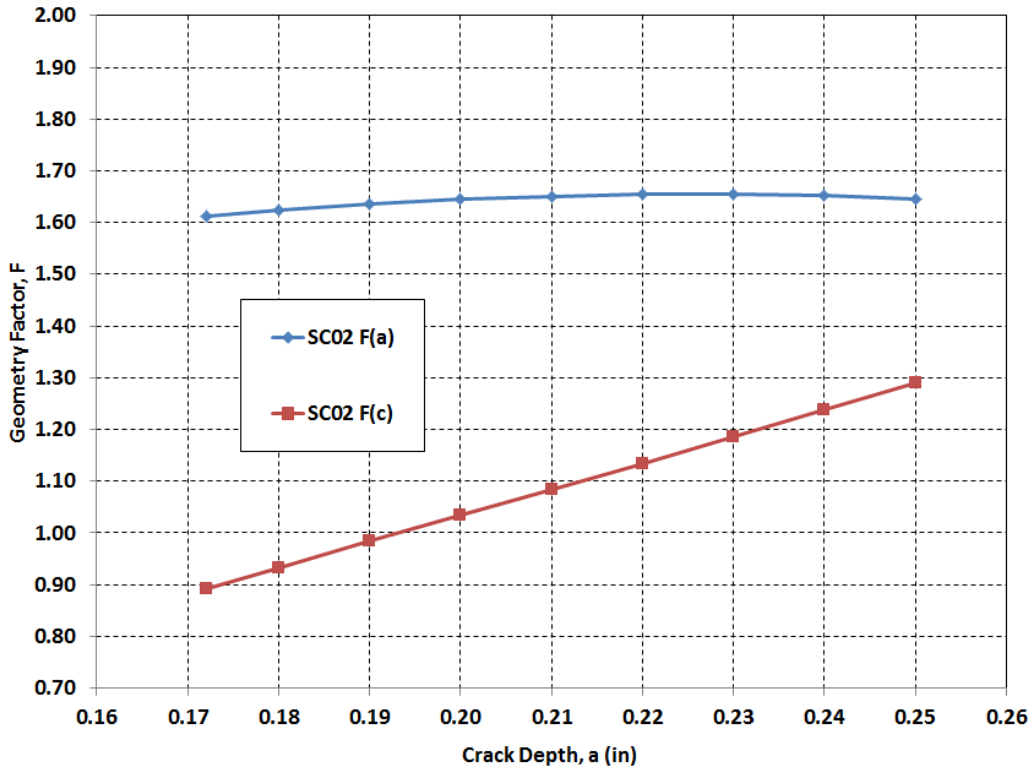

Figure 6-3. Geometry Factors at the Crack Depth, F(a), and the Crack Surface, F(c), for the Stress Gradient in the Outer Shell Layer as a Function of Crack Depth, as Computed Using NASGRO Model SC02

Table 6-1. Tabulated Values of Geometry Factors F(a) and F(c)

Crack Depth a (in)	Half Surface Crack Length c (in)	Depth to Thickness Ratio a/t	Crack Aspect Ratio a/c	Geometry Factors	
				SC02 F(a)	SC02 F(c)
0.172	1.0	0.66	0.172	1.612	0.892
0.18	1.0	0.69	0.18	1.624	0.933
0.19	1.0	0.73	0.19	1.636	0.984
0.20	1.0	0.77	0.20	1.645	1.035
0.21	1.0	0.81	0.21	1.651	1.085
0.22	1.0	0.85	0.22	1.655	1.135
0.23	1.0	0.88	0.23	1.655	1.186
0.24	1.0	0.92	0.24	1.652	1.238
0.25	1.0	0.96	0.25	1.646	1.290

7.0 FATIGUE CRACK GROWTH ANALYSIS

This section first provides a review of fatigue crack growth (FCG) data and how they are modeled using the NASGRO equation [10]. While the NASGRO software contains some data for these materials from the 1975 NASA Langley report [2], these data sets are not as extensive as one would hope and exhibit considerable scatter (see Figures 5-11 and 5-12). The FCG data generated in this Phase 1 effort was first compared to a Paris equation from Barsom [11] quoted for these materials in the Langley report. A set of NASGRO equation parameters for the 1146a shell material was obtained using the NASMAT module of NASGRO and was then used to perform an analysis of the fatigue crack growth from the notch in the outer shell layer that occurred during the cyclic pressure testing.

7.1 Fatigue Crack Growth Rate Data Background

Fatigue crack growth rate data are generally characterized on log-log plots of growth rate, da/dN (in/cycle) versus stress intensity factor range, ΔK (ksi$\sqrt{}$in). It is commonplace to consider FCG data to be divided into three regions as shown schematically in Figure 7-1. Region I is the fatigue "threshold" region where cracks propagate very slowly and the data usually exhibit a threshold (ΔK_{th}) below which cracks do not propagate. Region II is the linear or steady-state region where the relationship between da/dN and ΔK is linear on a log-log plot. Region II is also commonly referred to as the Paris region after the power law equation [$da/dN = C(\Delta K)^n$] that has been used to model fatigue crack growth in this region for many years. Region III is the near instability region where rapid unstable crack growth occurs as fracture instability is approached.

Crack growth rate calculations in NASGRO use a relationship called the NASGRO equation given by:

$$\frac{da}{dN} = C\left[\left(\frac{1-f}{1-R}\right)\Delta K\right]^n \frac{\left(1-\frac{\Delta K_{th}}{\Delta K}\right)^p}{\left(1-\frac{K_{\max}}{K_c}\right)^q} \tag{7.1}$$

where N is the number of applied fatigue cycles, a is the crack length, R is the stress ratio, ΔK is the stress intensity factor range, and C, n, p, and q are empirically derived constants. The NASGRO equation is a "full-range" crack growth model in that it can represent all three crack growth regions as well as account for the dependence of FCG rate on the stress ratio. Closure is modeled using the Newman crack opening function, f. For additional detail on the NASGRO equation, the reader is referred to the documentation for the NASGRO software [10].

7.2 Fatigue Crack Growth Equations

Figure 7-2 plots all the fatigue crack growth data obtained in this Phase 1 effort for both the 1146a shell material and the A-225 Gr B head material (similar to Figure 5-11). For fatigue crack growth in ferrite-pearlite steels, Barsom [11] developed an "upper bound" Paris equation that the Langley report recommended be used [2]:

$$da/dN = 3.6\text{E-}10\ (\Delta K)^{3.0} \qquad (7.2)$$

This relationship is also shown plotted in Figure 7-2 for comparison and matches the data reasonably well; however, the slope is somewhat shallower than the measured data (above the data at low ΔK and below the data at higher ΔK (although as previously noted, these higher data are considered invalid). It does not appear that this equation is an upper bound over the full range of ΔK. The maximum ΔK used in developing this equation was about 60 ksi√in [11].

To fit the NASGRO equation to fatigue crack growth rate data, one generally needs multiple sets of data at different R values. In this Phase 1 effort, FCG rate data were obtained only at an R of 0.15; further testing at a higher R value has been recommended for Phase 2 to determine the extent of the variation on da/dN as a function of R. This variation is anticipated to be small but testing is required to verify this expectation.

However, in order to facilitate the FCG analysis of the crack that propagated out of the notch during the pressure testing, the NASGRO equation was fit to the 1146a shell FCG data (using only the single R value of 0.15). The resulting fit is shown in Figure 7-3 along with the corresponding NASGRO equation parameters. Note that a toughness value of 90 ksi√in was used in the fit (reference Table 5-3) and also that only the "valid" FCG data were used in the fit. The plot shows the NASGRO equation fit at R=0.15 and it matches the R=0.15 test data quite well. Also shown on the plot are the NASGRO equation lines computed for R=0 (blue) and R=0.45 (red); these R values correspond to the minimum and maximum R values that occurred in the cyclic pressure testing.

7.3 Pressure Vessel Cycle History

Digital Wave Corporation provided SwRI a spreadsheet containing the history of the internal pressures cycles that occurred during the testing. A total of 4688 pressure cycles were applied to the vessel over a period from September 2011 to March 2012. Based on communications with Digital Wave, each day the test began from zero pressure and the minimum pressure for the first cycle of each day was set to zero. The spreadsheet pressure history data were edited to account for this reality. Appendix A provides a listing of the pressure history and Figure 7-4 is a plot of the stress history in ksi for the outer layer computed using the same procedure as discussed in Section 6.1. In this figure the blue line represents the minimum stress in a cycle and the red line represents the maximum stress in a cycle. Figure 7-5 is a histogram of the R values contained in the pressure history indicating that the overwhelming majority of the cycles had R values between 0.1 and 0.2 (which was the reason the FCG rate testing was performed at R=0.15).

7.4 Analysis of FCG at Notch in Outer Shell

NASGRO was used to perform a fatigue crack growth analysis at the notch in the 1146a outer shell material. The fracture mechanics model used in the FCG analysis was the SC02 surface crack in a plate model and was identical to that described in Section 6.0, including the univariant through-thickness stress gradient. The initial flaw size for the analysis had a depth, a, of 0.172 inches and a total length, 2c, of 2.0 inches with an initial aspect ratio, a/c, of 0.172. The width , W, was 24 inches and the thickness, t, was 0.26 inches.

Two crack growth analyses were performed. The first used the NASGRO equation fit to the R=0.15 da/dN data shown in Figure 7-3. The second analysis used the Barsom equation discussed above (Eqn. 7.2). The material data input screens captured from the NASGRO GUI for each of these cases are shown in Figures 7-6 and 7-7, respectively. In each of these cases, the NASGRO user-defined material option was employed. In the case of the Barsom (Paris) model, the base formulation of the NASGRO equation (Eqn. 7.1) was simplified by setting p=q=0 and removing (suppressing) closure in order to obtain a linear (Paris model). In each case the values of fracture toughness, yield strength, and ultimate strength used were the average values listed in Section 4.0.

Plots of crack depth and crack length for each analysis are shown in Figures 7-8 and 7-9, respectively, where the red curve represents the crack depth, a, and the green curve represents the surface crack half-length, c. Table 7-1 provides a summary of the results. Both analyses predict failure of the fatigue crack prior to the end of the total number of pressure cycles that were applied in the test (N_{test} = 4,688 cycles); however, the NASGRO equation analysis predicts a shorter life to failure. Both analyses predicted small amounts of crack growth along the surface.

Table 7-1. Results of Fatigue Crack Growth Analysis

FCG Material Model	Nthru (cycles)	Nf (cycles)	Nthru/Ntest	Nf/Ntest	Comments
NASGRO Equation	3,674 a = 0.260 c = 1.012	4,582 c = 1.353	0.78	0.98	surface crack transitioned to through crack before failure occurred
Barsom Equation	4,661 a = 0.257 c = 1.020	4,661 c = 1.020	0.99	0.99	surface crack failed by fracture, transitioned to through crack, and failed immediately

Notes:
(1) Ntest is the total number of pressure cycles during the test (4,688).
(2) Nthru is the number of cycles to a through crack.
(3) Nf is the number of cylces at failure by fracture.
(4) Crack sizes are in units of inches.

The analysis performed using the NASGRO equation predicts that the surface crack will transition to a through crack (without failure) at 3,674 cycles (N_{thru}) and continue growing as a through crack until failure (N_f) after 4,582 cycles. In this analysis, the transition to the through crack occurred at load step number 201 (pressure = 8.4 ksi) and failure occurred at load step number 258 (pressure = 10 ksi). This failure is sooner than what happened in the test for the actual crack and (from Figure 4-1 and the fracture surface analysis) the ligament ahead of the fatigue crack was shown by examination of the fracture surface to fail by rapid fracture.

In contrast, the analysis using the Barsom equation comes very close to the end of the test predicting failure after 4,661 cycles. In this case the surface crack failed by fracture at cycle

4,662 and upon transition to a through crack, was predicted to fail immediately as a through crack. Cycle number 4,662 was the first cycle at an internal maximum pressure of 14 ksi and as show in Section 6.2, this corresponded to a stress intensity factor of 85.6 ksi√in, nearly reaching the average fracture toughness of 90 ksi√in. Again, this leads to the conclusion that the rapid fracture observed on the fracture surface most likely occurred at one of the 14 ksi pressure cycles near the very end of the test.

The fractographic analysis (Section 4.0) showed that regions of fatigue striations were evident at various locations on the crack surface. Crack growth rate estimates obtained from the striation spacings ranged from 7.2×10^{-6} inch/cycle near the notch to 1.8×10^{-5} inch/cycle adjacent to the transition to fast fracture. For comparison to these measurements, Figures 7-10 and 7-11 plot the computed crack growth rates da/dN and dc/dN for the analysis using the NASGRO equation and the Barsom equation, respectively. The striation measurements correspond primarily to crack propagation in the through-thickness direction and can be compared to the red curves in Figures 7-10 and 7-11. In both analyses, the computed early crack growth rates bound the measured spacing of 7.2×10^{-6} inch/cycle. However, crack growth rates computed just before failure or transition of the surface crack are somewhat higher than the measured spacing of 1.8×10^{-5} inch/cycle but they are of the same order of magnitude.

7.5 Discussion and Conclusions

The notch that was inserted into the outer shell layer of the multilayer vessel, although shallow (a/c = 0.17), was really quite large since it was 70 percent through the thickness of the shell (a/t = 0.172/0.26 = 0.70). Thus, at the beginning of the test (with a 6.6 ksi internal pressure), the stress intensity factor (and ΔK for the R=0 cycles) was about 34 ksi√in which is quite high on the FCG curve, approaching Region III, and near where the validity of the measured FCG rates in the material property characterization tests begins to come in to question. Since the Barsom equation at these stress intensity levels lies below the measured FCG data (and the NASGRO equation curve fit), it is therefore not surprising that it predicts longer life than the NASGRO equation analysis. Some of the difference between the two analytical predictions may also be a result of the stress ratio dependence built into the NASGRO equation. As previously mentioned, this could be better defined by conducting FCG testing at a higher R value, perhaps at R=0.5, but it is recognized (from Figure 7-5) that only about 10 percent of the cycles in the test were at a higher R.

The crack growth rates measured from the striation spacings can also be used in combination with the FCG data to estimate the applied ΔK and indicate that the applied ΔKs were at least 30 ksi√in, consistent with the values computed in the analyses.

Lastly, it is important to note that these analyses of the notch and the pressure test took place on the upper end of the FCG curve (approaching Region III) and that different conclusions could be possible if the crack size and stress history resulted in a spectrum that had a significant amount of cycles at lower ΔKs. For example, the Barsom equation crosses the FCG data (see Figure 7-2) and may actually be too conservative at lower ΔKs, particularly if the loading history results in a significant amount of cycles that would occur in or near the threshold region. For this reason, it is recommended that the full range of the FCG curve be characterized. And, as a practical matter, for cracks that start small, the majority of life is consumed at the lower crack growth rates and ΔKs further warranting a model such as the NASGRO equation that can account for behavior near the FCG threshold.

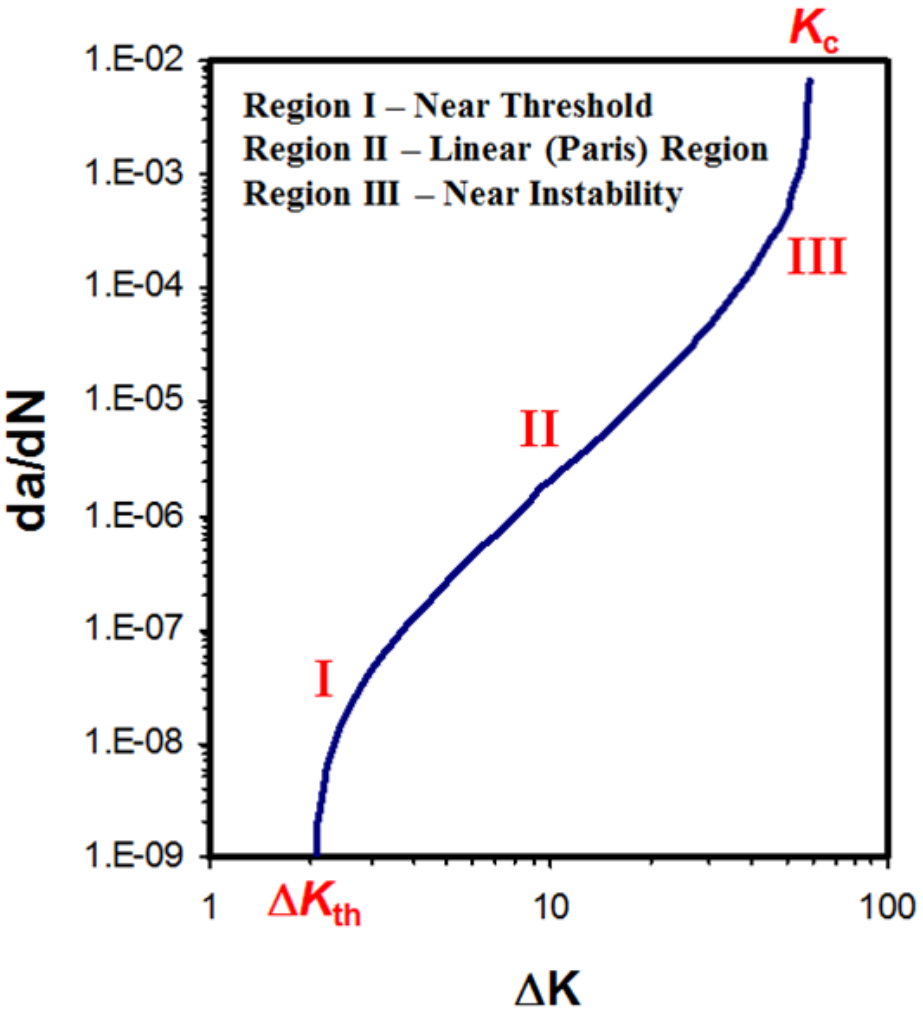

Figure 7-1. Schematic of Fatigue Crack Growth Behavior Illustrating the Three Regions of Fatigue Crack Growth

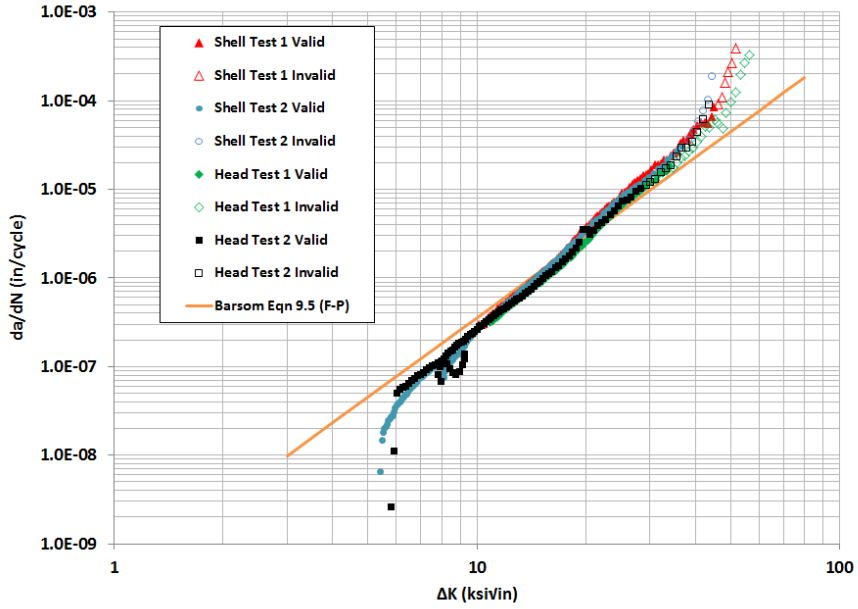

Figure 7-2. Comparison of Shell and Head FCG Data with Barsom Equation for Ferrite-Pearlite Steels

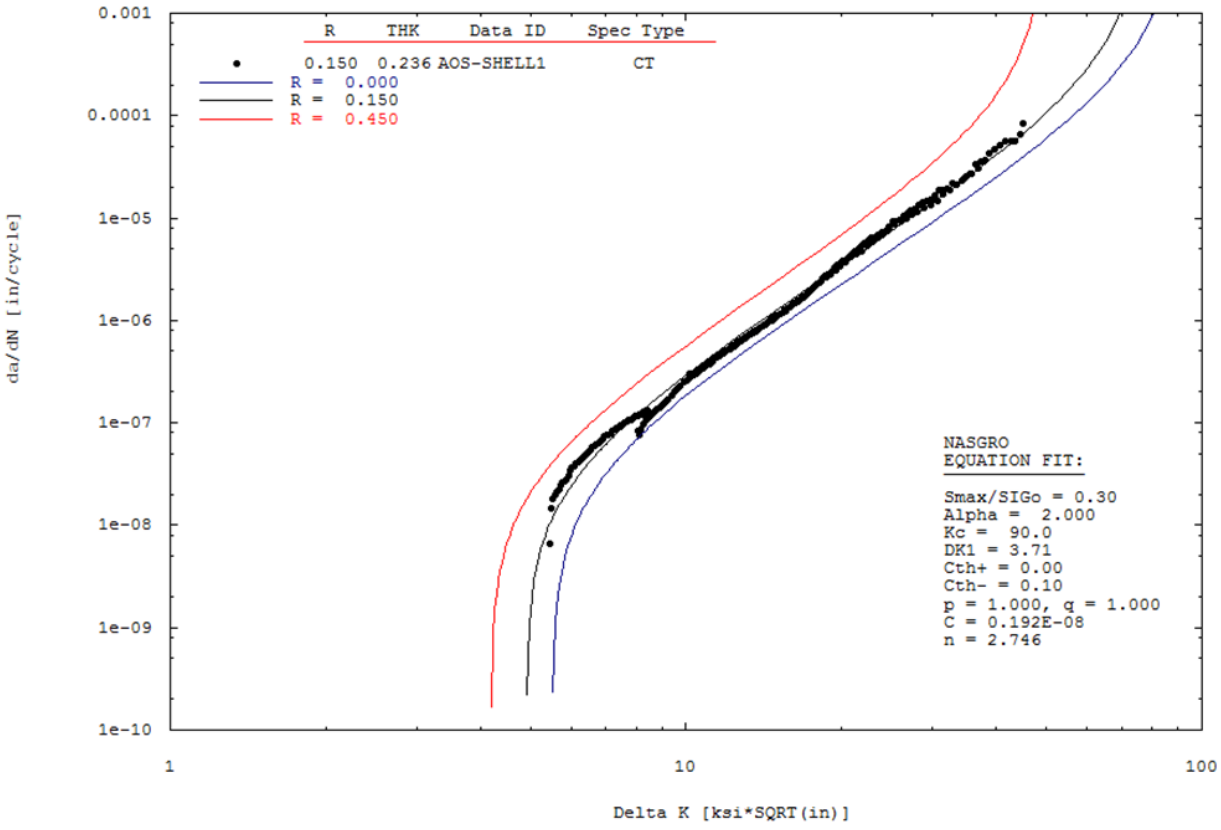

Figure 7-3. NASGRO Equation Fit to 1146a Shell FCG Data

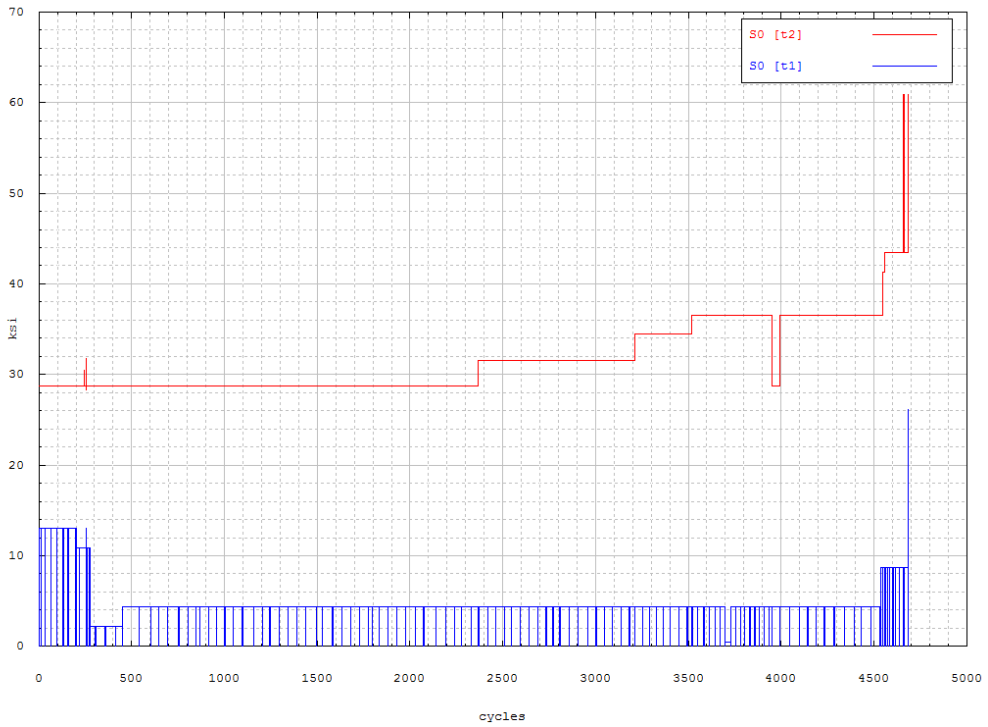

Figure 7-4. Stress History in Pressure Vessel Used in FCG Analysis

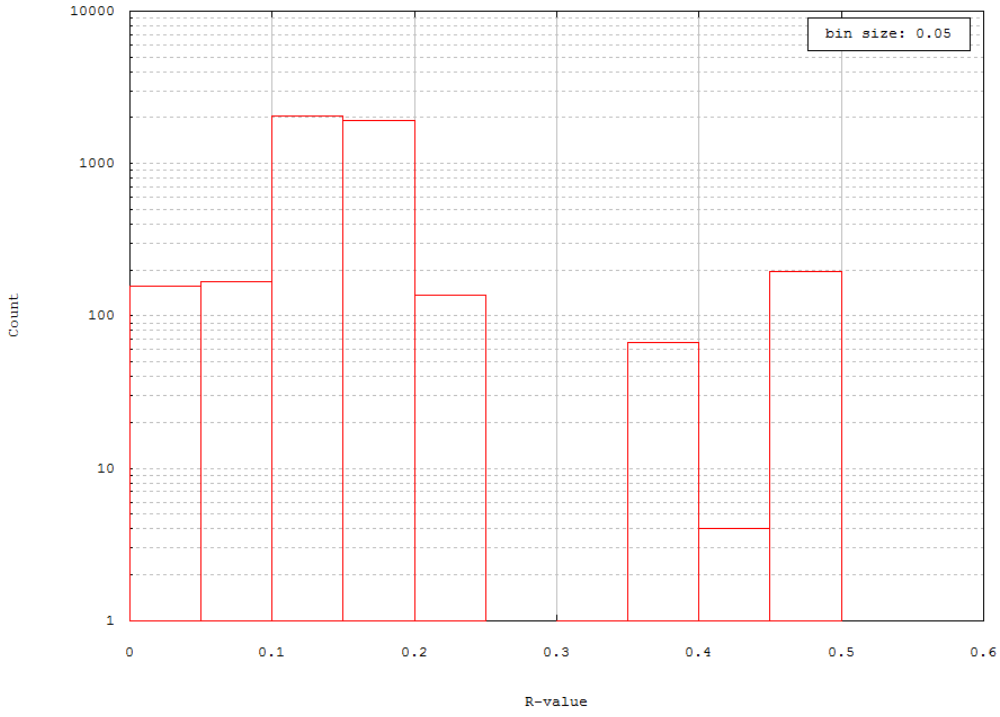

Figure 7-5. Histogram of R-Value Occurrences in Pressure Vessel Cycles

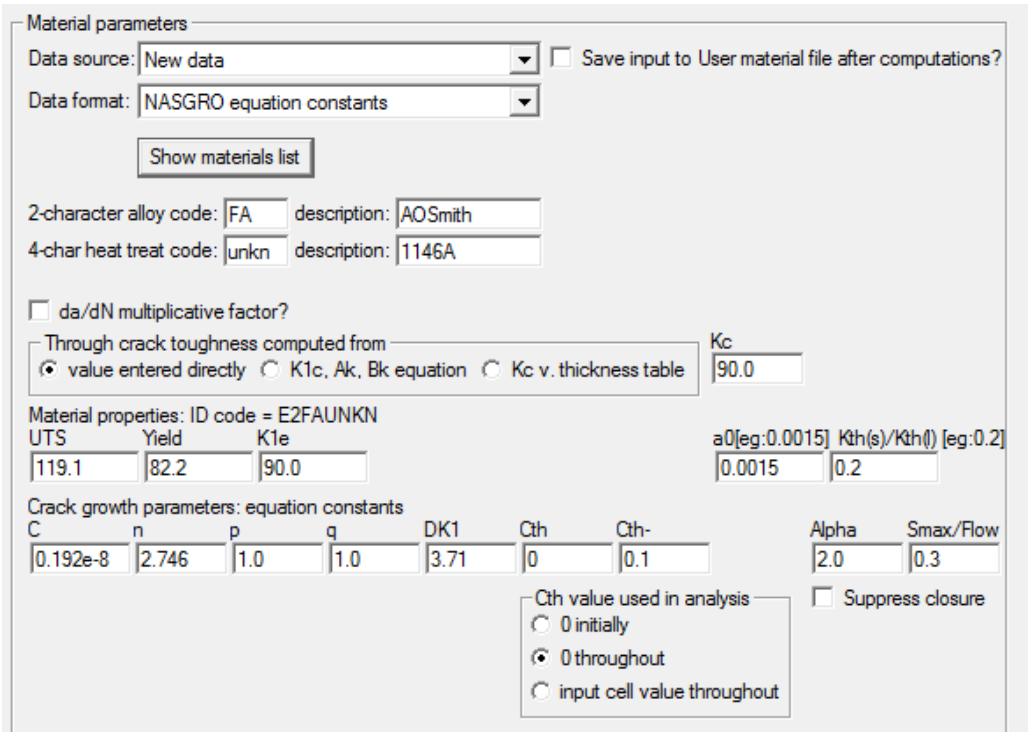

Figure 7-6. NASGRO Input Screen for NASGRO Equation Based on Curve Fit to 1146a FCG Data Obtained at R = 0.15

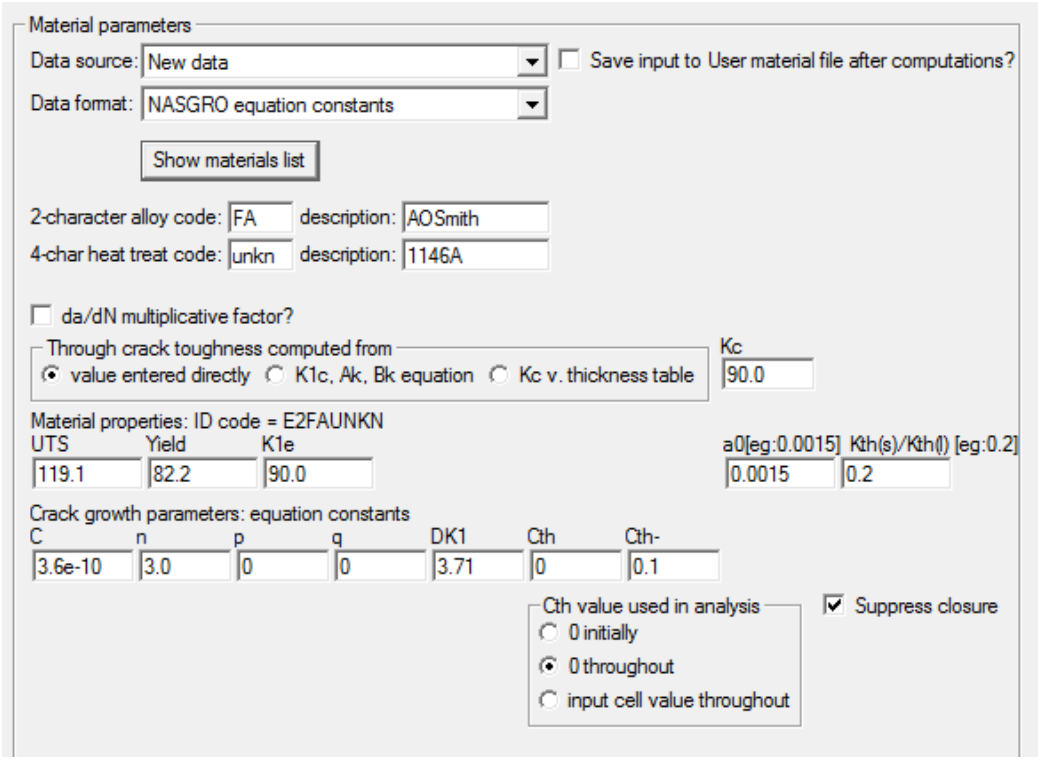

Figure 7-7. NASGRO Input Screen for Barsom Equation

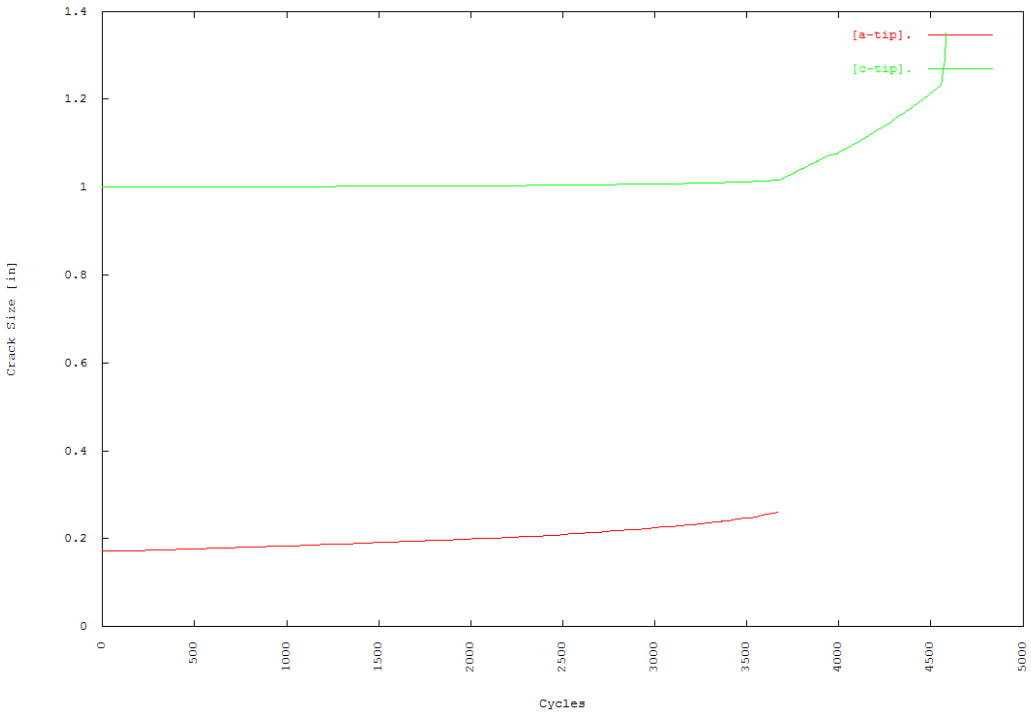

Figure 7-8. Crack Growth Curves Predicted Using NASGRO Equation and SC02

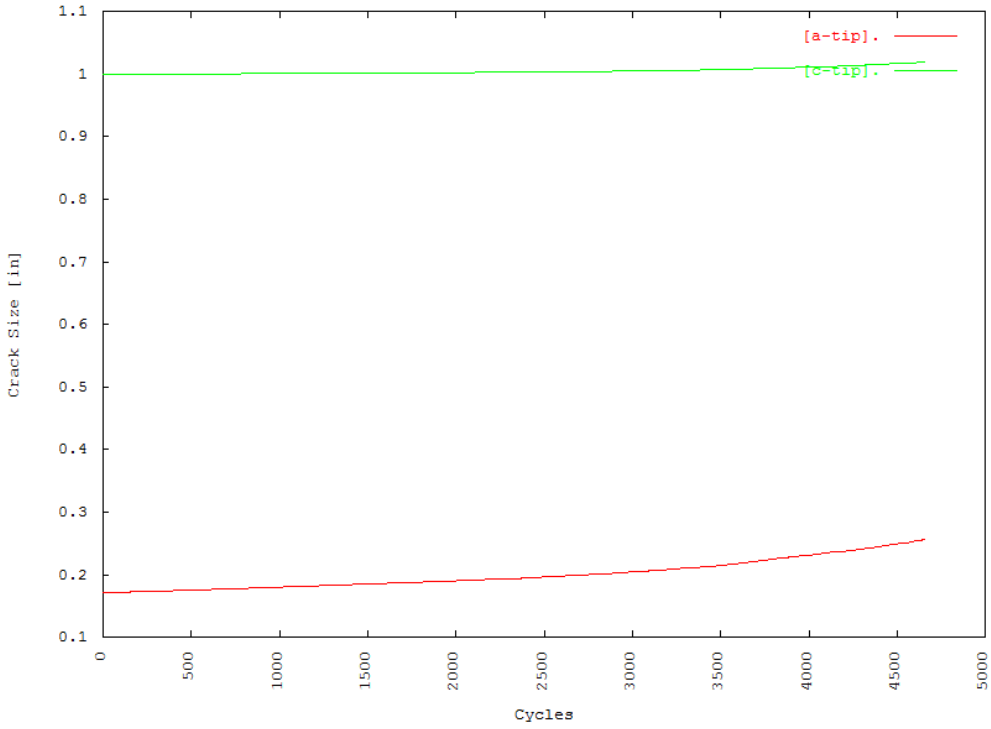

Figure 7-9. Crack Growth Curves Predicted Using Barsom Equation and SC02

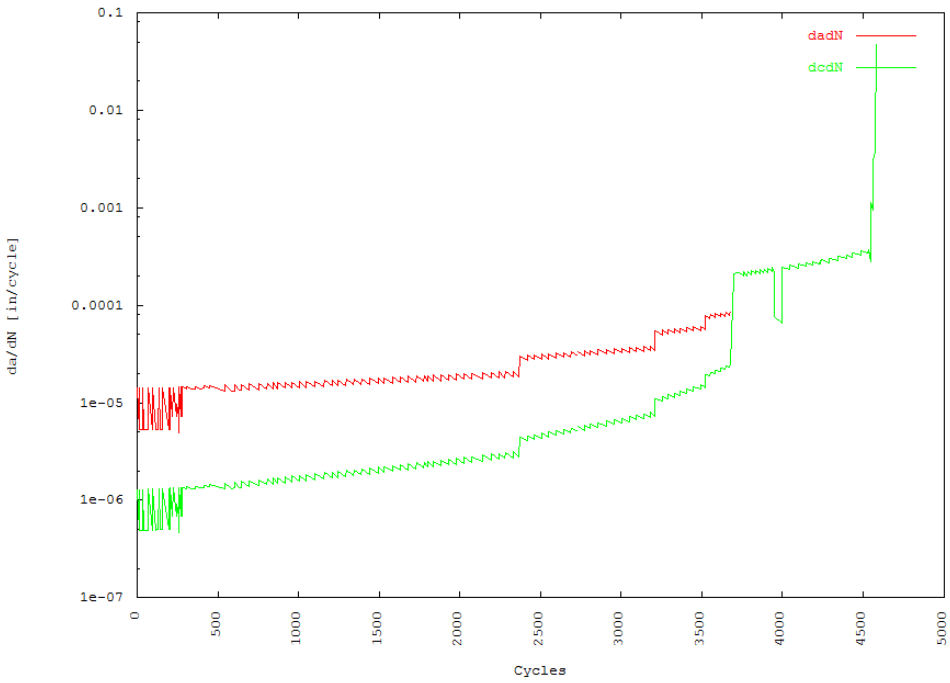

Figure 7-10. Crack Growth Rates Computed Using the NASGRO Equation

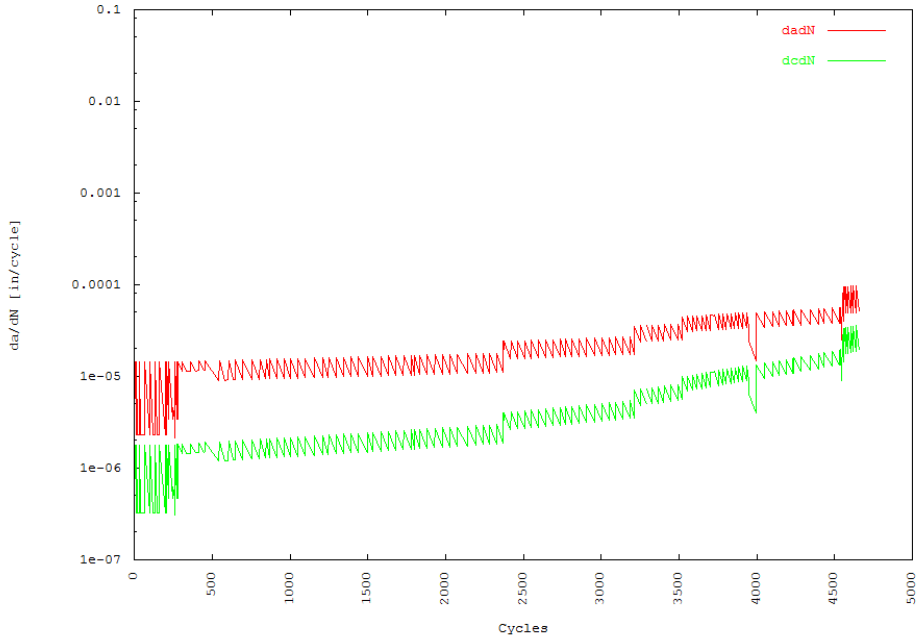

Figure 7-11. Crack Growth Rates Computed Using the Barsom Equation

8.0 REFERENCES

[1] ASTM E8, "Standard Test Methods for Tension Testing of Metallic Materials," Vol. 03.01, ASTM International, West Conshohocken, PA, 2010.

[2] C.M. Hudson, J.C. Newman, Jr., and P.E. Lewis, NASA Technical Memorandum, "An Investigation of Fracture Toughness, Fatigue Crack Growth, and Impact Properties of Three Pressure Vessel Steels," NASA TM X-3316, NASA LaRC, Hampton, VA, December, 1975.

[3] ASTM E23, "Standard Test Methods for Notched Bar Impact Testing of Metallic Materials," Vol. 03.01, ASTM International, West Conshohocken, PA, 2010.

[4] Towers, O. "Testing Sub Size Charpy Specimens – Parts 1, 2 and 3," Metal Construction, March, April, and May, 1986.

[5] API RP 579/ASME FFS-1, Fitness-For-Service, API Recommended Practice 579, Second Edition, American Petroleum Institute, Washington, D.C., June 2007.

[6] ASTM E399, "Standard Test Method for Linear-Elastic Plane-Strain Fracture Toughness K_{Ic} of Metallic Materials," Vol. 03.01, ASTM International, West Conshohocken, PA, 2010.

[7] ASTM E561, "Standard Test Method for K-R Curve Determination," Vol. 03.01, ASTM International, West Conshohocken, PA, 2010.

[8] ASTM E1820, "Standard Test Method for Measurement of Fracture Toughness," Vol. 03.01, ASTM International, West Conshohocken, PA, 2010.

[9] ASTM E647, "Standard Test Method for Measurement of Fatigue Crack Growth Rates," Vol. 03.01, ASTM International, West Conshohocken, PA, 2010.

[10] NASGRO® Fracture Mechanics and Fatigue Crack Growth Analysis Software, Version 6.21, Southwest Research Institute and NASA Johnson Space Center, January 2012.

[11] Barsom, J.M. and Rolfe, S.T., *Fracture and Fatigue Control in Structures: Applications of Fracture Mechanics*, Third Edition, ASTM, West Conshohocken, PA, 1999.

Appendix A: Pressure Vessel Cycle History

NASGRO Step Number	Minimum Pressure (ksi)	Maximum Pressure (ksi)	Number of Cycles	Cumulative Number of Cycles
1	0.0	6.6	1	1
2	3.0	6.6	9	10
3	0.0	6.6	1	11
4	3.0	6.6	4	15
5	3.0	6.6	4	19
6	3.0	6.6	10	29
7	3.0	6.6	2	31
8	0.0	6.6	1	32
9	3.0	6.6	8	40
10	3.0	6.6	5	45
11	3.0	6.6	20	65
12	0.0	6.6	1	66
13	3.0	6.6	29	95
14	0.0	6.6	1	96
15	3.0	6.6	18	114
16	3.0	6.6	17	131
17	0.0	6.6	1	132
18	3.0	6.6	12	144
19	3.0	6.6	2	146
20	3.0	6.6	11	157
21	0.0	6.6	1	158
22	3.0	6.6	38	196
23	0.0	6.6	1	197
24	3.0	6.6	3	200
25	3.0	6.6	2	202
26	0.0	6.6	1	203
27	2.5	6.6	16	219
28	0.0	6.6	1	220
29	2.5	6.6	24	244
30	2.5	7.0	1	245
31	2.5	6.6	10	255
32	2.5	7.3	1	256
33	3.0	6.5	1	257
34	0.0	6.6	1	258
35	2.5	6.6	12	270
36	0.0	6.6	1	271
37	2.5	6.6	1	272
38	0.0	6.6	1	273
39	2.5	6.6	3	276
40	0.0	6.6	1	277
41	0.5	6.6	28	305

NASGRO Step Number	Minimum Pressure (ksi)	Maximum Pressure (ksi)	Number of Cycles	Cumulative Number of Cycles
42	0.0	6.6	1	306
43	0.5	6.6	24	330
44	0.5	6.6	28	358
45	0.0	6.6	1	359
46	0.5	6.6	31	390
47	0.5	6.6	23	413
48	0.0	6.6	1	414
49	0.5	6.6	32	446
50	0.5	6.6	3	449
51	0.0	6.6	1	450
52	1.0	6.6	92	542
53	0.0	6.6	1	543
54	1.0	6.6	37	580
55	1.0	6.6	22	602
56	0.0	6.6	1	603
57	1.0	6.6	31	634
58	1.0	6.6	12	646
59	0.0	6.6	1	647
60	1.0	6.6	44	691
61	0.0	6.6	1	692
62	1.0	6.6	62	754
63	0.0	6.6	1	755
64	1.0	6.6	49	804
65	0.0	6.6	1	805
66	1.0	6.6	39	844
67	0.0	6.6	1	845
68	1.0	6.6	24	869
69	0.0	6.6	1	870
70	1.0	6.6	44	914
71	0.0	6.6	1	915
72	1.0	6.6	44	959
73	0.0	6.6	1	960
74	1.0	6.6	42	1002
75	0.0	6.6	1	1003
76	1.0	6.6	44	1047
77	0.0	6.6	1	1048
78	1.0	6.6	49	1097
79	0.0	6.6	1	1098
80	1.0	6.6	59	1157
81	0.0	6.6	1	1158
82	1.0	6.6	49	1207
83	0.0	6.6	1	1208

NASGRO Step Number	Minimum Pressure (ksi)	Maximum Pressure (ksi)	Number of Cycles	Cumulative Number of Cycles
84	1.0	6.6	37	1245
85	0.0	6.6	1	1246
86	1.0	6.6	47	1293
87	0.0	6.6	1	1294
88	1.0	6.6	47	1341
89	0.0	6.6	1	1342
90	1.0	6.6	46	1388
91	0.0	6.6	1	1389
92	1.0	6.6	48	1437
93	0.0	6.6	1	1438
94	1.0	6.6	58	1496
95	0.0	6.6	1	1497
96	1.0	6.6	32	1529
97	0.0	6.6	1	1530
98	1.0	6.6	53	1583
99	0.0	6.6	1	1584
100	1.0	6.6	47	1631
101	0.0	6.6	1	1632
102	1.0	6.6	48	1680
103	0.0	6.6	1	1681
104	1.0	6.6	47	1728
105	0.0	6.6	1	1729
106	1.0	6.6	47	1776
107	0.0	6.6	1	1777
108	1.0	6.6	20	1797
109	0.0	6.6	1	1798
110	1.0	6.6	35	1833
111	0.0	6.6	1	1834
112	1.0	6.6	47	1881
113	0.0	6.6	1	1882
114	1.0	6.6	47	1929
115	0.0	6.6	1	1930
116	1.0	6.6	48	1978
117	0.0	6.6	1	1979
118	1.0	6.6	48	2027
119	0.0	6.6	1	2028
120	1.0	6.6	46	2074
121	0.0	6.6	1	2075
122	1.0	6.6	65	2140
123	0.0	6.6	1	2141
124	1.0	6.6	51	2192
125	0.0	6.6	1	2193

NASGRO Step Number	Minimum Pressure (ksi)	Maximum Pressure (ksi)	Number of Cycles	Cumulative Number of Cycles
126	1.0	6.6	47	2240
127	0.0	6.6	1	2241
128	1.0	6.6	38	2279
129	0.0	6.6	1	2280
130	1.0	6.6	49	2329
131	0.0	6.6	1	2330
132	1.0	6.6	38	2368
133	0.0	7.3	1	2369
134	1.0	7.3	2	2371
135	0.0	7.3	1	2372
136	1.0	7.3	46	2418
137	0.0	7.3	1	2419
138	1.0	7.3	42	2461
139	0.0	7.3	1	2462
140	1.0	7.3	48	2510
141	0.0	7.3	1	2511
142	1.0	7.3	36	2547
143	0.0	7.3	1	2548
144	1.0	7.3	46	2594
145	0.0	7.3	1	2595
146	1.0	7.3	47	2642
147	0.0	7.3	1	2643
148	1.0	7.3	44	2687
149	0.0	7.3	1	2688
150	1.0	7.3	46	2734
151	0.0	7.3	1	2735
152	1.0	7.3	36	2771
153	0.0	7.3	1	2772
154	1.0	7.3	36	2808
155	0.0	7.3	1	2809
156	1.0	7.3	47	2856
157	0.0	7.3	1	2857
158	1.0	7.3	49	2906
159	0.0	7.3	1	2907
160	1.0	7.3	50	2957
161	0.0	7.3	1	2958
162	1.0	7.3	45	3003
163	0.0	7.3	1	3004
164	1.0	7.3	45	3049
165	0.0	7.3	1	3050
166	1.0	7.3	42	3092
167	0.0	7.3	1	3093

NASGRO Step Number	Minimum Pressure (ksi)	Maximum Pressure (ksi)	Number of Cycles	Cumulative Number of Cycles
168	1.0	7.3	44	3137
169	0.0	7.3	1	3138
170	1.0	7.3	45	3183
171	0.0	7.3	1	3184
172	1.0	7.3	26	3210
173	0.0	7.9	1	3211
174	0.0	7.9	1	3212
175	1.0	7.9	41	3253
176	0.0	7.9	1	3254
177	1.0	7.9	38	3292
178	0.0	7.9	1	3293
179	1.0	7.9	35	3328
180	0.0	7.9	1	3329
181	1.0	7.9	34	3363
182	0.0	7.9	1	3364
183	1.0	7.9	38	3402
184	0.0	7.9	1	3403
185	1.0	7.9	45	3448
186	0.0	7.9	1	3449
187	1.0	7.9	45	3494
188	0.0	7.9	1	3495
189	1.0	7.9	25	3520
190	0.0	8.4	1	3521
191	1.0	8.4	30	3551
192	0.0	8.4	1	3552
193	1.0	8.4	32	3584
194	0.0	8.4	1	3585
195	1.0	8.4	30	3615
196	0.0	8.4	1	3616
197	1.0	8.4	30	3646
198	0.0	8.4	1	3647
199	1.0	8.4	26	3673
200	0.0	8.4	1	3674
201	1.0	8.4	25	3699
202	0.0	8.4	1	3700
203	0.1	8.4	28	3728
204	0.0	8.4	1	3729
205	1.0	8.4	27	3756
206	0.0	8.4	1	3757
207	1.0	8.4	25	3782
208	0.0	8.4	1	3783
209	1.0	8.4	21	3804

NASGRO Step Number	Minimum Pressure (ksi)	Maximum Pressure (ksi)	Number of Cycles	Cumulative Number of Cycles
210	0.0	8.4	1	3805
211	1.0	8.4	27	3832
212	0.0	8.4	1	3833
213	1.0	8.4	25	3858
214	0.0	8.4	1	3859
215	1.0	8.4	25	3884
216	0.0	8.4	1	3885
217	1.0	8.4	25	3910
218	0.0	8.4	1	3911
219	1.0	8.4	25	3936
220	0.0	8.4	1	3937
221	1.0	8.4	14	3951
222	0.0	6.6	1	3952
223	1.0	6.6	42	3994
224	0.0	8.4	1	3995
225	1.0	8.4	51	4046
226	0.0	8.4	1	4047
227	1.0	8.4	53	4100
228	0.0	8.4	1	4101
229	1.0	8.4	43	4144
230	0.0	8.4	1	4145
231	1.0	8.4	42	4187
232	0.0	8.4	1	4188
233	1.0	8.4	43	4231
234	0.0	8.4	1	4232
235	1.0	8.4	6	4238
236	0.0	8.4	1	4239
237	1.0	8.4	47	4286
238	0.0	8.4	1	4287
239	1.0	8.4	55	4342
240	0.0	8.4	1	4343
241	1.0	8.4	52	4395
242	0.0	8.4	1	4396
243	1.0	8.4	35	4431
244	0.0	8.4	1	4432
245	1.0	8.4	54	4486
246	0.0	8.4	1	4487
247	1.0	8.4	43	4530
248	0.0	8.4	1	4531
249	1.0	8.4	4	4535
250	0.0	8.4	1	4536
251	2.0	8.4	12	4548

NASGRO Step Number	Minimum Pressure (ksi)	Maximum Pressure (ksi)	Number of Cycles	Cumulative Number of Cycles
252	0.0	9.5	1	4549
253	2.0	9.5	11	4560
254	0.0	10.0	1	4561
255	0.0	10.0	1	4562
256	2.0	10.0	11	4573
257	0.0	10.0	1	4574
258	2.0	10.0	9	4583
259	0.0	10.0	1	4584
260	2.0	10.0	19	4603
261	0.0	10.0	1	4604
262	2.0	10.0	13	4617
263	0.0	10.0	1	4618
264	2.0	10.0	21	4639
265	0.0	10.0	1	4640
266	2.0	10.0	21	4661
267	0.0	14.0	1	4662
268	0.0	10.0	1	4663
269	2.0	10.0	20	4683
270	0.0	14.0	1	4684
271	6.0	14.0	4	4688

REPORT DOCUMENTATION PAGE

Form Approved
OMB No. 0704-0188

1. REPORT DATE *(DD-MM-YYYY)*	2. REPORT TYPE	3. DATES COVERED *(From - To)*
01- 01 - 2014	Contractor Report	

4. TITLE AND SUBTITLE
Multilayer Pressure Vessel Materials Testing and Analysis
Phase I

5a. CONTRACT NUMBER
NNA09DB39C

5b. GRANT NUMBER

5c. PROGRAM ELEMENT NUMBER

6. AUTHOR(S)
Cardinal, Joseph W.; Popelar, Carl F.; Page, Richard A.

5d. PROJECT NUMBER
OSMA SMA Project 724297

5e. TASK NUMBER

5f. WORK UNIT NUMBER
724297.20.21.01.03

7. PERFORMING ORGANIZATION NAME(S) AND ADDRESS(ES)
NASA Langley Research Center
Hampton, VA 23681-2199

8. PERFORMING ORGANIZATION REPORT NUMBER

9. SPONSORING/MONITORING AGENCY NAME(S) AND ADDRESS(ES)
National Aeronautics and Space Administration
Washington, DC 20546-0001

10. SPONSOR/MONITOR'S ACRONYM(S)
NASA

11. SPONSOR/MONITOR'S REPORT NUMBER(S)
NASA/CR-2014-218157

12. DISTRIBUTION/AVAILABILITY STATEMENT
Unclassified - Unlimited
Subject Category 39 Structural Mechanics
Availability: NASA CASI (443) 757-5802

13. SUPPLEMENTARY NOTES
Publication of this report was requested by the NESC. This task was funded by OSMA in with funds transferred to ARC for program execution. Doug Fraser was the NASA Project Manager at ARC. Jacobs ATOM managed the project through their contracts office under NASA contract NNA09DB39C. Owen Greulich and Doug Fraser were the NASA Technical Monitors.

14. ABSTRACT

To provide NASA a comprehensive suite of materials strength, fracture toughness and crack growth rate test results for use in remaining life calculations for aging multilayer pressure vessels, Southwest Research Institute® (SwRI®) was contracted in two phases to obtain relevant material property data from a representative vessel. This report describes Phase 1 of this effort which includes a preliminary material property assessment as well as a fractographic, fracture mechanics and fatigue crack growth analyses of an induced flaw in the outer shell of a representative multilayer vessel that was subjected to cyclic pressure test. SwRI performed this Phase 1 effort under contract to the Digital Wave Corporation in support of their contract to Jacobs ATOM for the NASA Ames Research Center.

15. SUBJECT TERMS
Modal Acoustic Emission; Crack Growth Rate; Pressure Vessel; Fatigue crack growth

16. SECURITY CLASSIFICATION OF:			17. LIMITATION OF ABSTRACT	18. NUMBER OF PAGES	19a. NAME OF RESPONSIBLE PERSON
a. REPORT	b. ABSTRACT	c. THIS PAGE			STI Help Desk (email: help@sti.nasa.gov)
					19b. TELEPHONE NUMBER *(Include area code)*
U	U	U	UU	73	(443) 757-5802